

# Climatic effects of surface albedo geoengineering

Peter J. Irvine,<sup>1</sup> Andy Ridgwell,<sup>1</sup> and Daniel J. Lunt<sup>1</sup>

Received 20 May 2011; revised 5 October 2011; accepted 6 October 2011; published 22 December 2011.

[1] Various surface albedo modification geoengineering schemes such as those involving desert, urban, or agricultural areas have been proposed as potential strategies for helping counteract the warming caused by greenhouse gas emissions. However, such schemes tend to be inherently limited in their potential and would create a much more heterogeneous radiative forcing than propositions for space-based “reflectors” and enhanced stratospheric aerosol concentrations. Here we present results of a series of atmosphere–ocean general circulation model (GCM) simulations to compare three surface albedo geoengineering proposals: urban, cropland, and desert albedo enhancement. We find that the cooling effect of surface albedo modification is strongly seasonal and mostly confined to the areas of application. For urban and cropland geoengineering, the global effects are minor but, because of being colocated with areas of human activity, they may provide some regional benefits. Global desert geoengineering, which is associated with significant global-scale changes in circulation and the hydrological cycle, causes a smaller reduction in global precipitation per degree of cooling than sunshade geoengineering,  $1.1\% \text{ K}^{-1}$  and  $2.0\% \text{ K}^{-1}$  respectively, but a far greater reduction in the precipitation over land,  $3.9\% \text{ K}^{-1}$  compared with  $1.0\% \text{ K}^{-1}$ . Desert geoengineering also causes large regional-scale changes in precipitation with a large reduction in the intensity of the Indian and African monsoons in particular. None of the schemes studied reverse the climate changes associated with a doubling of CO<sub>2</sub>, with desert geoengineering profoundly altering the climate and with urban and cropland geoengineering providing only some regional amelioration at most.

**Citation:** Irvine, P. J., A. Ridgwell, and D. J. Lunt (2011), Climatic effects of surface albedo geoengineering, *J. Geophys. Res.*, 116, D24112, doi:10.1029/2011JD016281.

## 1. Introduction

[2] The Intergovernmental Panel on Climate Change (IPCC) Fourth Assessment Report concluded that the global temperature change by 2100 would likely range from  $1.1^\circ\text{C}$  to  $6.4^\circ\text{C}$ , depending on the climate sensitivity of the Earth and on the emissions pathway followed [Intergovernmental Panel on Climate Change (IPCC), 2007]. To limit global warming to  $2^\circ\text{C}$  or less, a target proposed by the European Union [Commission of European Communities, 2007], some authors predict that emissions reductions of 90% by 2050 would be required [Weaver *et al.*, 2007]. However, efforts to mitigate carbon emissions so far have been relatively ineffectual; global emissions of greenhouse gases increased by 29% between 2000 and 2008 to  $8.7 \text{ Pg C yr}^{-1}$ , reduced in 2009 by 1.3% as a result of the economic crisis and are projected to have grown during 2010 by more than 3% [Friedlingstein *et al.*, 2010; Le Quéré *et al.*, 2009].

[3] Solar radiation management (SRM) geoengineering, or “climate engineering,” a proposed means to tackle future climate change [Shepherd *et al.*, 2009], involves increasing

the upward (toward space) reflection of sunlight and reducing the fraction of shortwave radiation absorbed at the surface, hence cooling the climate and potentially countering the warming effects of increased CO<sub>2</sub> (and other greenhouse gases). Increasing the outgoing shortwave radiation can, in theory, be achieved through increasing the albedo at a number of different heights in the atmosphere, at the surface, or even in space. This flexibility over which mediums could be modified and over which areas the modification could be applied has led to a wide variety of SRM schemes being proposed, such as of the creation of a sunshade in space [Angel, 2006], cloud albedo modification [Salter *et al.*, 2008], and stratospheric injection of sulfate aerosols [Crutzen, 2006], together with a number of surface albedo geoengineering schemes, including crop albedo enhancement [Ridgwell *et al.*, 2009], urban albedo enhancement [Akbari *et al.*, 2009], and desert albedo geoengineering [Gaskill, 2004].

[4] Most attention to date has been on cloud and aerosol SRM schemes because of their potential to be deployed on a quasi-global scale and to exert sufficient forcing to cancel anthropogenic greenhouse warming of up to a doubling of CO<sub>2</sub> [Shepherd *et al.*, 2009]. Space-based reflectors also fall into this category, but because of the high cost and very long deployment time scale [Angel, 2006] they have attracted less serious consideration. In contrast, surface

<sup>1</sup>Bristol Research Initiative for the Dynamic Global Environment, School of Geographical Sciences, University of Bristol, Bristol, UK.

albedo modification (SAM) geoengineering schemes would generally be deployed rather more heterogeneously across the Earth's surface and, because of their more limited potential for global impact [Shepherd *et al.*, 2009], have been less well studied. In this paper we address the climate consequences of the three principal SAM schemes: urban areas, croplands, and deserts.

[5] In the rest of section 1 we outline the three land SAM schemes that are the focus of this paper. We do not investigate whether the schemes outlined are economically or technologically feasible options for geoengineering; rather we adopt the schemes as they are described in the literature and then simulate the effects that these schemes have on the climate of an atmospheric-ocean general circulation model (AOGCM).

### 1.1. Urban Albedo Geoengineering

[6] The idea of urban albedo geoengineering has been considered for a number of years in the guise of reducing the heat island effect and helping improve air quality in cities [Pomerantz *et al.*, 1999; Taha *et al.*, 1999]. Urban albedo geoengineering involves enhancing the albedo of urban areas by replacing standard building materials, for roofs and paving, etc., with alternative more reflective (higher-albedo) materials or by adding a more reflective coating [Akbari *et al.*, 2009; Bretz *et al.*, 1998]. Achievable increases in the albedo of roofing and paving of 0.1–0.4 and 0.15–0.25, respectively, have been estimated, equivalent to an average increase in urban albedo of 0.1 [Akbari *et al.*, 2009]. An alternative estimate of the potential increase in albedo of 0.15 was made by Hamwey [2007], which remains within the range considered by Akbari *et al.* [2009]. There is a larger range for the estimates of the fraction of the Earth's surface that is covered by suitable urban areas. Hamwey [2007] estimates the suitable urban area at 0.64% of the Earth's surface, from an assumed urban area per capita; Akbari *et al.* [2009] estimate 0.29% on the basis of the Global Rural-Urban Mapping Project (GRUMP) urban extent data set [Global Rural-Urban Mapping Project (GRUMP), 2005]; however, Lenton and Vaughan [2009] caution that other satellite data indicated the urban area could be as low as 0.051% [Hansen *et al.*, 2000; Loveland *et al.*, 2000]. We take the estimates of potential albedo increase and urban extent from Akbari *et al.* [2009] as the basis for our simulations because of the availability of the GRUMP data set and the moderate estimate of potential albedo increase.

### 1.2. Crop Albedo Geoengineering

[7] Biogegeoengineering or crop albedo geoengineering would involve growing crop plant varieties with a higher albedo than currently grown as a means to produce a cooling of the planet. Crop albedo is often higher than the albedo of natural vegetation, for example, barley, at European latitudes, has a higher albedo (0.23) than deciduous (0.18) or coniferous (0.16) woodland [Monteith and Unsworth, 1990]. Hence the spread of agriculture has historically led to a modification of the albedo properties of the Earth's surface [Betts *et al.*, 2007; Costa *et al.*, 2007], which has cooled the Earth by an estimated 0.17°C [Matthews *et al.*, 2003]. The albedo of different varieties of a single crop species also differs, depending on, for example, the properties of the leaf wax, the "hairiness" of the leaves and the morphology of the

leaf canopy [Febrero *et al.*, 1998; Hatfield and Carlson, 1979; Holmes and Keiller, 2002]. It has been proposed that these properties could be managed to increase the overall albedo of both grassland (pasture) [Hamwey, 2007] and cropland [Ridgwell *et al.*, 2009], although recent analysis of a sample of soybean isolines concluded that existing variability may not be as great as previously assumed [Doughty *et al.*, 2011].

[8] There are various proposals for the types of areas suitable for crop albedo modification and a range of estimates for the potential increase in albedo. Hamwey [2007] suggests that all grassland (cropland, pasture, and wild grassland) could be modified and that the albedo could be increased by 25% (+0.0425), Lenton and Vaughan [2009] calculated that when applied to all grassland (~7.5% of the Earth's surface) a radiative forcing of  $-0.51 \text{ W m}^{-2}$  would be achieved. Ridgwell *et al.* [2009] and Doughty *et al.* [2011] propose only albedo increases to cropland and suggest albedo increases with ranges of 0.02–0.08 and 0.05–0.15, respectively. We adopt the range of Ridgwell *et al.* [2009] as it represents a midsized scheme and uses a similar model.

### 1.3. Desert Albedo Geoengineering

[9] Finally, desert albedo geoengineering involves the laying of highly reflective material across the extensive desert areas of the world to increase the average planetary albedo [Gaskill, 2004]. Suggestions for achieving this include laying and cleaning some form of reinforced plastic sheeting by automated vehicles, covering an estimated 11.7 million km<sup>2</sup> of suitable desert [Gaskill, 2004]. The area of deserts that could be suitable for this type of geoengineering cover ~2% of the Earth's surface, and the albedo increase proposed is from ~0.36 to ~0.8. This scheme would produce the greatest radiative forcing and cooling of the different surface albedo schemes compared in this paper [Lenton and Vaughan, 2009]. We adopt this scheme for desert albedo geoengineering, which represents the most extreme example of localized surface albedo modification suggested.

### 1.4. Summary and Paper Outline

[10] The three different proposals for surface albedo modification (SAM) geoengineering schemes considered here have been previously compared using zero-dimensional (0-D) or one-dimensional (1-D) radiative forcing calculations [for example, Lenton and Vaughan, 2009 and Hamwey, 2007]. However, unlike other climate engineering schemes, SAM geoengineering schemes would be deployed heterogeneously across the Earth's surface. Hence, one would expect important regional-scale impacts and potential side effects that may not be revealed by annual and global-scale averaging. While there have been several general circulation model (GCM) analyses made for urban albedo enhancement [Oleson *et al.*, 2010] and crop albedo enhancement [Ridgwell *et al.*, 2009; Singarayer *et al.*, 2009], these were made using different models and used different experimental and analysis methodologies (e.g., integration time), preventing direct comparison of their projections.

[11] To address this, we have carried out a GCM analysis of all three main SAM schemes, using the same model and the same methodology, presenting GCM results for desert geoengineering for the first time. This allows us to directly

compare the three schemes side by side and to explore the relative seasonal and regional impacts that will be very important for these spatially heterogeneous schemes.

[12] To compare the different schemes we analyze the global, local, and remote climate effects of regional surface albedo modification and assess the extent and “quality” of the climate change amelioration achieved. For an initial comparison we conduct an analysis of the effects of the schemes on precipitation and temperature at the global scale. To analyze the local cooling effect we focus on Europe, a region with large urban and crop areas, which is located near to the Sahara (and hence may be expected to be cooled significantly by desert albedo geoengineering). We also analyze the effect of the schemes on regional precipitation, focusing particularly on monsoon regions and analyzing some of the changes in circulation. For remote effects we focus on Arctic snow and sea-ice changes; the Arctic is a region remote from any of the regions affected by SAM but one that has been a focus for previous climate engineering studies [Caldeira and Wood, 2008; Irvine et al., 2009; Robock et al., 2008]. It must be noted that, while the results presented here are illustrative of the types of changes that could be expected, GCM models do not, in general, simulate precipitation or regional climate changes well [Cox et al., 2000; IPCC, 2007].

[13] This paper continues with a methodology, results section, and a discussion and conclusion section. Section 3 is split into global effects, European summer changes, monsoon changes, and Arctic changes. The discussion and conclusion will deal with the implications of the results presented.

## 2. Methodology

[14] HadCM3, the fully coupled atmosphere–ocean global circulation model (AOGCM) used in this paper [Gordon et al., 2000], has been used in the IPCC third and fourth assessment reports [IPCC, 2007] and performs well in a number of tests relative to other global GCMs [Covey et al., 2003; IPCC, 2007]. Although it has been superseded by HadGEM2 [Collins et al., 2011] for the fifth IPCC assessment and can no longer be considered “state-of-the-art,” HadCM3 does have the advantages of being relatively computationally efficient that allows more and/or longer runs to be conducted than would be possible with a more recent, higher-resolution model.

[15] The horizontal resolution of the atmospheric model is  $2.5^\circ$  in latitude by  $3.75^\circ$  in longitude, with 19 vertical layers. The atmospheric model has a time step of 30 min and includes many parameterizations representing subgrid-scale effects, such as convection [Gregory and Rowntree, 1990] and boundary layer mixing [Smith, 1993]. The land surface scheme includes the representation of the freezing and melting of soil moisture. The spatial resolution in the ocean is  $1.25^\circ \times 1.25^\circ$ , with 20 vertical layers. The ocean model component uses the Gent and McWilliams [1990] mixing scheme, and there is no explicit horizontal tracer diffusion. The sea-ice model uses a simple thermodynamic scheme and contains parameterizations of sea-ice drift and leads [Cattle and Crossley, 1995]. HadCM3 has a climate sensitivity of  $3.3^\circ\text{C}$  for a doubling of  $\text{CO}_2$ , which falls in the midrange of the estimate of the likely climate sensitivity reported in the IPCC AR4 ( $2.0^\circ\text{C}$ – $4.5^\circ\text{C}$ ) [Solomon et al., 2007].

[16] We employ the MOSES 1 land surface scheme [Cox et al., 1999], which accounts for terrestrial surface fluxes of temperature, moisture, and radiation. Although later versions of MOSES are available, for example Essery et al. [2003], the combination of HadCM3 with MOSES 1 is the most widely used and is the most robustly tested [Gordon et al., 2000; Johns et al., 2003; Martin et al., 2006] and for this reason we employ this combination. MOSES includes four soil layers, recording temperature, moisture and phase changes, a canopy layer, and a representation of snow cover. The representation of evaporation includes the dependence of stomatal resistance on temperature, vapor pressure, and  $\text{CO}_2$  concentration [Cox et al., 1999]. Each grid cell has surface properties; roughness length, snow-free albedo, etc., that reflect the vegetation cover present, as derived from the Wilson and Henderson-Sellers data set [Wilson and Henderson-Sellers, 1985].

[17] In the simulations presented here we modified the albedo properties in MOSES, i.e., snow-free albedo and deep-snow albedo, in areas that would be affected by the different surface albedo geoengineering schemes considered. All other surface properties were left fixed at preindustrial conditions for all experiments. We carried out 11 different model simulations using HadCM3: a preindustrial simulation, a simulation with doubled preindustrial  $\text{CO}_2$  concentration ( $2 \times \text{CO}_2$ ), plus nine simulations with increased surface albedo and doubled  $\text{CO}_2$ , consisting of three simulations with increased albedo for each of the three geoengineering schemes (urban, crop, and desert albedo geoengineering). An additional simulation, with  $2 \times \text{CO}_2$  and a reduction in incoming solar radiation sufficient to return global average temperature to preindustrial levels (referred to as sunshade geoengineering), was run for comparison. This sunshade geoengineering was achieved by reducing the solar constant by a fraction sufficient to return the global average temperature to the preindustrial value; in our case a 2.1% reduction in incoming sunlight was required (this is the same method implemented by Lunt et al. [2008] and Irvine et al. [2009]).

[18] The regions over which the increases in albedo were applied for each of the schemes are shown in Figure 1. The area for the urban and crop albedo schemes remained the same for each simulation, with the degree of albedo increase varying. For the desert geoengineering simulations, the albedo increase remained the same for all simulations but the areas modified were varied (Figure 1). Table 1 summarizes the albedo modifications and area coverage of all the different geoengineering scenarios considered here. In most of our analysis we focus on the maximum implementation of each scheme. We do not suggest that these are the most feasible or likely implementations, but were chosen to give the strongest and hence most statistically significant change in order to help identify any subtle effects. All model runs were initialized from a preindustrial spin-up totaling more than 1000 years with each simulation being run for a total of 400 years, using the final 100 years for averaging.

### 2.1. Urban Albedo Modification

[19] Urban albedo geoengineering has the smallest potential radiative forcing of the three different SRM interventions

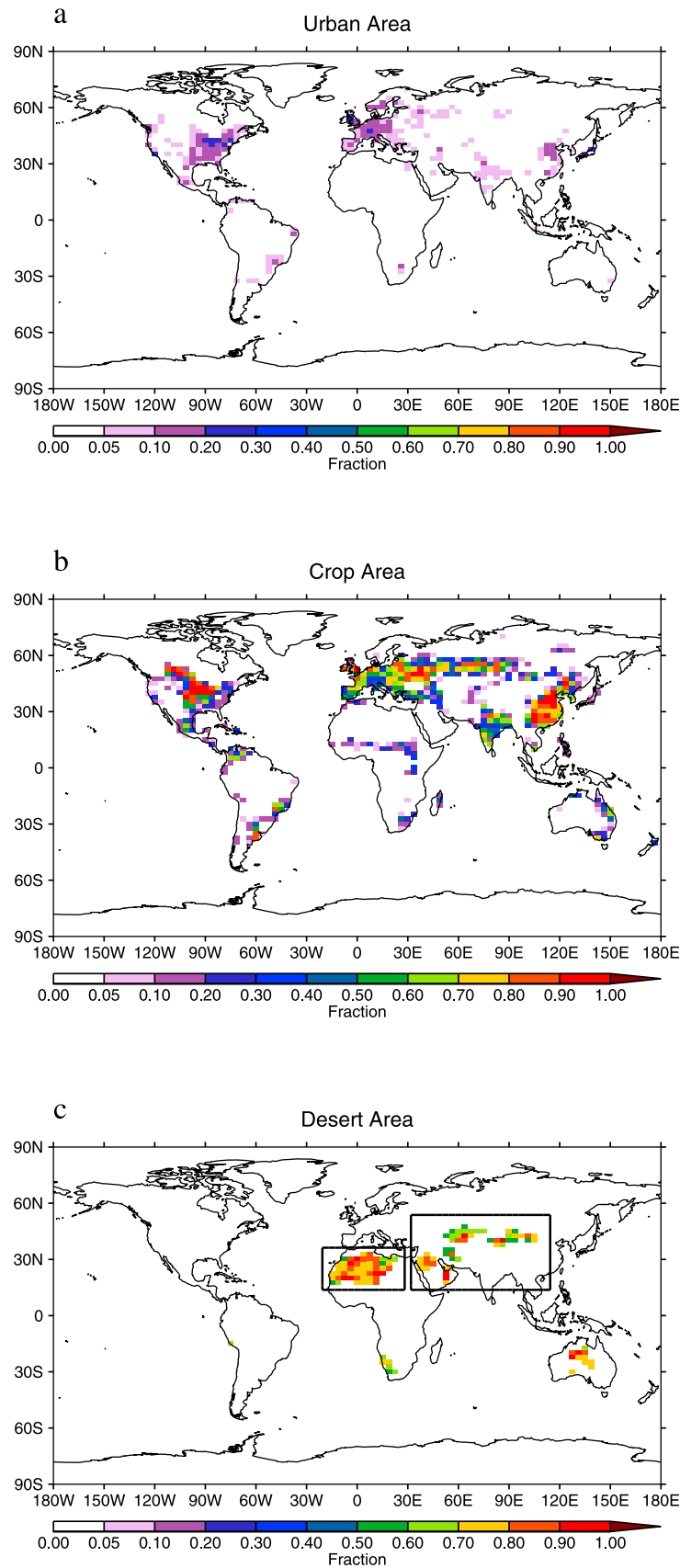


**Figure 1.** Maps showing the fractional coverage of (a) urban, (b) crop, and (c) desert to which albedo increases were applied. The boxes in 1c show the limited domains of albedo enhancement for the Asian and Saharan desert schemes.

**Table 1.** Area Affected and Albedo Increase for Geoengineering Schemes

Geoengineering	Fractional Global Area (%)	Snow-Free Albedo Increase	Deep Snow Albedo Increase
Urban High	0.556	0.175	0.113
Urban Mid	0.556	0.1	0.0646
Urban Low	0.556	0.0725	0.046
Crops High	3.08	0.08	0
Crops Mid	3.08	0.04	0
Crops Low	3.08	0.02	0
Global Deserts	1.78	Set to 0.8	0
Asian Deserts	0.66	Set to 0.8	0
Sahara Desert	0.84	Set to 0.8	0

considered here, and in a previous GCM analysis no statistically significant changes in the climate were recorded [Oleson et al., 2010]. To test whether any feasible implementation of urban albedo enhancement would even be observable (let alone provide significant climate mitigation) and to allow us to fully elucidate the characteristics of the resulting changes in climate, we assumed an upper estimate of the area to which increased albedo could be applied. In this, we used the Global Rural-Urban Mapping Project (GRUMP) data set of urban extent [GRUMP, 2005] to determine the fraction of each model grid cell that is “urban.” The total urban area recorded in the GRUMP urban extent map is  $3.5 \times 10^6 \text{ km}^2$ , or 0.68% of the Earth’s area, which, after regressing onto the HadCM3 land grid (Figure 1b), becomes  $2.8 \times 10^6 \text{ km}^2$ , or 0.56% of the Earth’s area (and 1.9% of total land area). The difference is a consequence of the relatively low resolution of HadCM3 and consequent loss of some coastal urban areas in the gridding process.

[20] We followed the methodology of Akbari et al. [2009], assuming 35% of the urban area is paved and 25% is roofing, and applied albedo enhancement to these two surfaces, leaving the other 40% unchanged. From the estimates of Akbari et al. [2009], we tested three levels of albedo increases to roofing and paving (which on average have an albedo estimated at around 0.2 and 0.1, respectively): (1) a maximum increase of 0.35 and 0.25, respectively, (2) a moderate increase of 0.25 and 0.15, respectively, and (3) a small increase of 0.15 and 0.1, respectively. The overall increase in snow-free albedo applied is shown in Table 1. Urban areas at higher latitudes are often snow covered in winter months and so a change to the deep-snow albedo in the model was also applied (Table 1). The effect of albedo increases in urban areas will affect the deep-snow albedo but only insofar as the underlying surface is exposed. Although the MOSES 1 land surface scheme [Cox et al., 1999] used here does not have an urban land type, MOSES 2.2 does [Essery et al., 2003]. We hence used the values for snow-free and deep-snow albedo from MOSES 2.2 to calculate the exposed fraction:

$$\alpha_{us} = f \cdot \alpha_u + (1 - f) \alpha_s,$$

where  $\alpha_{us}$  is the recorded deep-snow albedo of urban areas,  $f$  is the fraction of exposed urban surface,  $1 - f$  is the fraction of snow coverage,  $\alpha_u$  is the snow-free urban albedo, and  $\alpha_s$  is the deep-snow albedo in the open. In MOSES 1, deep-snow  $\alpha_s$  has an albedo of 0.8, and the urban albedo values from MOSES 2.2 are 0.4 for  $\alpha_{us}$  and 0.18 for  $\alpha_u$

[Wiscombe and Warren, 1980]. On this basis,  $f$  was found to be 0.645, and so the deep-snow albedo increase applied to urban areas is  $f(\Delta\alpha_u)$ ; the full list of albedo modifications can be found in Table 1.

## 2.2. Crop Albedo Modification

[21] Crop albedo geoengineering has been tested in HadCM3 by Ridgwell et al. [2009] and Singarayer et al. [2009] and in CAM 3.0 by Doughty et al. [2011]. We follow a methodology similar to that of both Ridgwell et al. [2009] and Singarayer et al. [2009], apart from using the MOSES 1 land surface scheme rather than MOSES 2.1, used in these studies, in order to provide consistency with the other simulations presented in this paper. We adopt the same definition of crop extent, with the crop area being defined as C3 or C4 grasses that are within human-controlled or disturbed areas as defined by the Wilson and Henderson-Sellers [1985] land-type data set. The total area covered by crops is  $15.7 \times 10^6 \text{ km}^2$ , 3.1% of the Earth’s surface area or 10.6% of the land area (Figure 1a). To these areas we apply an increase in snow-free albedo dependent on the fractional crop coverage in the grid cell.

[22] We test the same albedo increases as Ridgwell et al. [2009] did, +0.02, +0.04, +0.08, to provide a point of direct comparison. Ridgwell et al. [2009] argue that these levels span the range of changes of what could be possible within existing intervariety albedo variability. This range is consistent with measurements of the leaf albedo of wheat and sorghum that exhibit variations of 0.05 and 0.16, respectively, between varieties [Grant et al., 2003; Uddin and Marshall, 1988]. An average canopy albedo increase of 0.04 in commercially grown varieties may thus be at least partially achievable using traditional plant-breeding techniques. However, in the analysis of a number of soybean isolines, Doughty et al. [2011] found differences in albedo no greater than our lowest tested assumption (+0.02). The deep-snow albedo was not modified as crop coverage is at very low levels in snowy conditions, assuming that either crop plants are not present (or exist as planted seeds) or have minimal canopy during the winter months.

## 2.3. Desert Albedo Modification

[23] Desert geoengineering represents the most extreme local albedo modification of the surface albedo modification schemes considered, and we explore the effects of different spatial extents instead of exploring different levels (intensities) of implementation. In an account of a U.S. Department of Energy (DOE) meeting on geoengineering, Gaskill [2004] estimates a possible albedo of 0.8 for commercially available coverings and that an estimated  $11.7 \times 10^6 \text{ km}^2$  would be suitable for this application. We take these estimates as the basis for our extreme case of what is possible for desert geoengineering.

[24] We generated a definition for desert areas, based on a combination of observed precipitation and fractional vegetation cover at the resolution of HadCM3, designed to roughly match the estimated total area of that given by Gaskill [2004]. If a grid cell receives on average precipitation of less than  $250 \text{ mm yr}^{-1}$ , as calculated from the CRU (Climate Research Unit, University of East Anglia) reanalysis data for the period 1961–1990, then it is classed as desert. We also specified that a grid cell must be less

**Table 2.** Annual Average Surface Air Temperature and Precipitation Change<sup>a</sup>

Experiments	Global		Land	
	SAT (°C)	Precipitation (%)	SAT (°C)	Precipitation (%)
2 × CO <sub>2</sub> , Preindustrial	<b>3.03</b>	<b>3.99</b>	<b>4.16</b>	<b>1.84</b>
Urban High, 2 × CO <sub>2</sub>	<b>-0.11</b>	-0.07	<b>-0.21</b>	0.18
Urban Mid, 2 × CO <sub>2</sub>	<b>-0.06</b>	-0.03	<b>-0.12</b>	0.33
Urban Low, 2 × CO <sub>2</sub>	-0.05	-0.04	<b>-0.10</b>	0.20
Crops High, 2 × CO <sub>2</sub>	<b>-0.23</b>	-0.20	<b>-0.42</b>	-0.07
Crops Mid, 2 × CO <sub>2</sub>	<b>-0.14</b>	0.09	<b>-0.26</b>	0.17
Crops Low, 2 × CO <sub>2</sub>	-0.05	0.01	<b>-0.11</b>	0.12
Global Deserts, 2 × CO <sub>2</sub>	<b>-1.12</b>	<b>-1.19</b>	<b>-2.20</b>	<b>-4.33</b>
Sahara Desert, 2 × CO <sub>2</sub>	<b>-0.52</b>	<b>-0.69</b>	<b>-1.06</b>	<b>-3.38</b>
Asian Deserts, 2 × CO <sub>2</sub>	<b>-0.53</b>	-0.34	<b>-1.02</b>	1.13
Sunshade, 2 × CO <sub>2</sub>	<b>-2.91</b>	<b>-5.71</b>	<b>-3.86</b>	<b>-2.87</b>

<sup>a</sup>Boldface values passed a 5% student *t* test for statistical significance.

than 50% covered in vegetation, as defined by the Wilson and Henderson-Sellers land-type data set [Wilson and Henderson-Sellers, 1985], before it was considered suitable for desert geoengineering (Figure 1c). This simple method does not capture all desert regions (notably, no deserts are identified in North America) but our method does produce a total area (9.1 million km<sup>2</sup>) close to the estimate (11.7 million km<sup>2</sup>) of Gaskill [2004]. The albedos of the desert grid cells are adjusted to

$$\alpha = f\alpha_o + (1-f)0.8,$$

where the albedo  $\alpha$  is dependent on the vegetated fraction  $f$ ,  $\alpha_o$  is the original albedo of the grid cell, and 0.8 is the albedo of the reflective covering. The deep-snow albedo was not changed as the properties of snow deposited on a reflective coating would be similar to those of snow on desert regions.

[25] Three experiments were run to explore the effect of applying desert albedo geoengineering in different regions (see Figure 1c): (1) in which all desert regions were modified (“Global”), (2) modification of only the Sahara desert (“Sahara”), (3) in which only Asian deserts, i.e., from Saudi Arabia and the Middle East eastward, are modified (“Asian”).

### 3. Results

[26] We present results of the global, local, and remote climate effects of SAM geoengineering, splitting the results into four parts: global effects (section 3.1), European summertime changes (section 3.2), monsoon system changes (section 3.3), and Arctic changes (section 3.4). The global effects section gives an overview of the major changes in temperature and precipitation that arise because of the different geoengineering schemes.

[27] In addition to this global assessment of climate effects, a number of specific changes are investigated: Europe is an illustrative region as there is a high crop and urban density in the region and it is also relatively close to the Sahara, suggesting that we might expect some effect on European climate from each of the SAM geoengineering schemes. Monsoon systems are associated with seasonal atmospheric overturning circulations driven by land-sea temperature differences and play a central role in continental hydrology [Trenberth *et al.*, 2000]. We can expect that

SAM geoengineering will change the seasonal land-sea temperature difference that plays a key role in monsoon circulations, making this an essential part of our analysis. Climate change in the Arctic is expected to be greater than elsewhere because of the action of local positive climate feedbacks, e.g., the melting of snow and ice and the consequent albedo decrease [IPCC, 2007]; we examine the effect of SAM geoengineering schemes on the Arctic to assess their effectiveness at reversing the amplified climate change there. All values reported in the text have passed a 5% student *t*-test significance test unless otherwise stated.

[28] Throughout the results sections we focus on a common subset of the simulations, i.e., the simulations with largest albedo modifications for each surface albedo geoengineering scheme. This is because the weaker crop and urban geoengineering schemes induce relatively small changes in climate that can be difficult to distinguish from the model’s internal variability. However, in focusing on the extreme urban and crop geoengineering implementations, we do not claim that these changes in climate would necessarily be linear with respect to the magnitude of SAM albedo increase. For desert geoengineering the global implementation is shown in all figures, and the Asian and Saharan implementations are shown if space allows.

[29] In this study we mostly calculate climate anomalies relative to the 2 × CO<sub>2</sub> simulation rather than to the pre-industrial (“Pre-ind”) simulation. This makes it easy to see the small changes in climate brought about by urban and crop geoengineering, without their being dwarfed by the changes from 2 × CO<sub>2</sub> to preindustrial. For desert and sunshade geoengineering, we also compare with preindustrial, as the climate changes that these schemes can cause are large enough to reverse the effects of doubling CO<sub>2</sub> in some cases.

#### 3.1. Global Effects

[30] The impacts on global and land-averaged temperatures and precipitation for each geoengineering scheme, as well as the effect of unmitigated global warming, are summarized in Table 2. At doubled CO<sub>2</sub> there is a global average increase in surface air temperature of +3.0°C and an increase in precipitation of +4.0%. On land, the annual average temperature change is amplified (+4.2°C) whereas the precipitation enhancement is reduced (down to +1.8%). Global-average warming is not completely reversed by any SAM scheme, with urban geoengineering having the potential to cool on a global annual average basis by a maximum of 0.11°C, crop geoengineering by 0.23°C, and (global) desert geoengineering by 1.12°C, with the amount of cooling determined by the assumed degree of geoengineering intervention.

[31] Changes in the radiative forcing of the planet affect the hydrological cycle in two ways: There is a “slow” or temperature-driven component that does not depend on the details of the radiative forcing mechanism, and there is a “fast” atmospheric adjustment component that differs between radiative forcing mechanisms [Andrews *et al.*, 2010]. The slow temperature response has been found to cause around a 2%–3% change in precipitation for every degree Kelvin of temperature change, with precipitation increasing with rising temperatures [Lambert and Webb, 2008]. Our simulations show that sunshade geoengineering caused a 2.0% K<sup>-1</sup> reduction in precipitation, whereas global desert

geoengineering caused only a  $1.1\% \text{ K}^{-1}$  reduction (we exclude urban and crop geoengineering as a statistically significant change in global average precipitation was not found). For comparison, a study on cloud albedo geoengineering (which increases albedo over ocean areas only) caused a  $2.5\% \text{ K}^{-1}$  reduction in global average precipitation [Bala *et al.*, 2010]. The different global precipitation responses of these geoengineering schemes are a result of the differing availability of moisture for evaporation in the regions affected, i.e., ocean regions have an infinite supply of water for evaporation whereas the continents do not. Thus, the effect of a reduction in incoming sunlight on the surface energy budget of the ocean will consist of a change in the latent and sensible heat fluxes, leading to a large reduction in evaporation, whereas over the land this will consist mainly of a change in sensible heat flux, with a smaller reduction in global evaporation.

[32] However, the change in continental precipitation shows an opposite result to this global picture; desert geoengineering has the largest reduction at  $3.9\% \text{ K}^{-1}$ , sunshade geoengineering shows  $1\% \text{ K}^{-1}$ , and cloud albedo geoengineering shows  $0.9\% \text{ K}^{-1}$ . This difference in continental precipitation arises from changes in circulation that redistribute the precipitation. This change in distribution has a greater effect on continental precipitation than does the change in the atmospheric moisture availability that controls global precipitation.

[33] The patterns of annual mean surface temperature change are shown in Figure 2. For unmitigated climate change (Figure 2a), warming occurs everywhere, with greater warming toward the poles and over the land areas. As one would expect, SAM geoengineering does not produce a uniform cooling. Furthermore, in some areas, statistically significant warming (in addition to the impact of  $2 \times \text{CO}_2$ ) occurs under each of the different geoengineering interventions, probably as a result of changes in circulation patterns, i.e., diverting warm currents of air to high-latitude areas. An example of this is the Southern Ocean around Tasmania, which is warmer for all three SAM geoengineering schemes. In contrast, sunshade geoengineering produces a relatively uniform cooling across the world compared with the surface albedo geoengineering schemes, with land areas and high-latitude areas cooled more than others, reversing most of the warming from  $2 \times \text{CO}_2$ .

[34] For urban geoengineering, we find a statistically significant cooling across most continental areas. This is in contrast to the results of Oleson *et al.* [2010], who did not find any statistically significant cooling as a result of a global reduction in urban albedo. This difference is likely to be partly due to the more extreme implementation we have assumed (and focused on the results of), together with the greater urban coverage assumed in our data set. We have also employed a longer averaging period: 100 years here compared with 58 years in the simulations of Oleson *et al.* [2010], and hence we are better able to identify small changes in climate against the background of modeled interannual variability. We find the largest cooling in Europe, North America, and in the Arctic, a consequence of the relatively large urban coverage of both Europe and North America (Figure 1b). This regional cooling is amplified by positive cryospheric feedbacks operating in the high

latitudes, particularly because of changes in sea-ice extent (see section 3.4).

[35] Crop albedo geoengineering exhibits a pattern of cooling (Figure 2c) to a first order similar to urban geoengineering (Figure 2b), with most of the cooling occurring in the Northern Hemisphere. This similarity between crop and urban albedo is due to the coexistence of greatest crop cover and urban fraction (population) in most regions (Figures 1a and 1b). Consistent with the results of Singarayer *et al.* [2009], our results show that crop albedo geoengineering results in the greatest cooling across Eurasia and North America. We also find less cooling than may be expected in South and East Asia, an area with significant crop coverage, a result of an associated reduction in cloud cover in the region [Doughty *et al.*, 2011; Singarayer *et al.*, 2009]. Some warm anomalies are also induced, for example in the Barents Sea, but are not found consistently in the moderate or weak implementations of crop geoengineering and are therefore perhaps a result of long-term climate variability.

[36] Although global desert geoengineering has the potential to generate the largest global average cooling effect, this average masks the fact that most of the  $1.12^\circ\text{C}$  cooling is highly concentrated over the desert regions where the albedo increase is applied (compare Figures 2d and 1c). For example, global desert geoengineering causes some areas of the Sahara to be greater than  $10^\circ\text{C}$  cooler than in the preindustrial (Figure 2f). A pronounced general cooling of most continental areas, of between  $1.5^\circ\text{C}$  and  $2^\circ\text{C}$  over most of Eurasia and North America also occurs, with the notable exception being India, which becomes slightly warmer despite being proximal to a number of desert areas. This warming in India can be explained by cloud feedbacks with an  $\sim 10\%$  reduction in cloud cover in the region (not shown). As with crop and urban geoengineering, the Northern Hemisphere tends to be cooled more than the Southern Hemisphere, a simple consequence of the presence of much greater land coverage in the north.

[37] Sunshade geoengineering produces a much more uniform cooling than the SAM schemes, with noticeably greater cooling in the Northern Hemisphere and the Arctic (Figure 2e), but does not reproduce the preindustrial temperature distribution; with the low latitudes cooler than in the preindustrial and the high latitudes warmer (Figure 2g). This difference in temperature is due to the greenhouse forcing acting to slow the loss of heat, which warms the Arctic more, and the reduced solar forcing, which has a greater role in the energy budget at low latitudes, acting to cool the tropics.

[38] In contrast to the response of surface air temperature, which is strongest at the sites of SAM geoengineering, changes in precipitation are much more heterogeneous (Figure 3). Doubling  $\text{CO}_2$  leads to large regional changes in precipitation, with some areas becoming much drier, e.g., the Amazon, South Africa, and Australia, and others becoming much wetter, e.g., South Asia and equatorial Africa, but with an overall increase in precipitation (see Figure 3a and Table 2). For both urban and crop albedo geoengineering, only minimal shifts in precipitation occur, with the exception of equatorial Pacific regions (Figures 3b and 3c), whereas desert geoengineering induces quite extreme changes in precipitation patterns throughout the tropics and subtropics (Figure 3d).

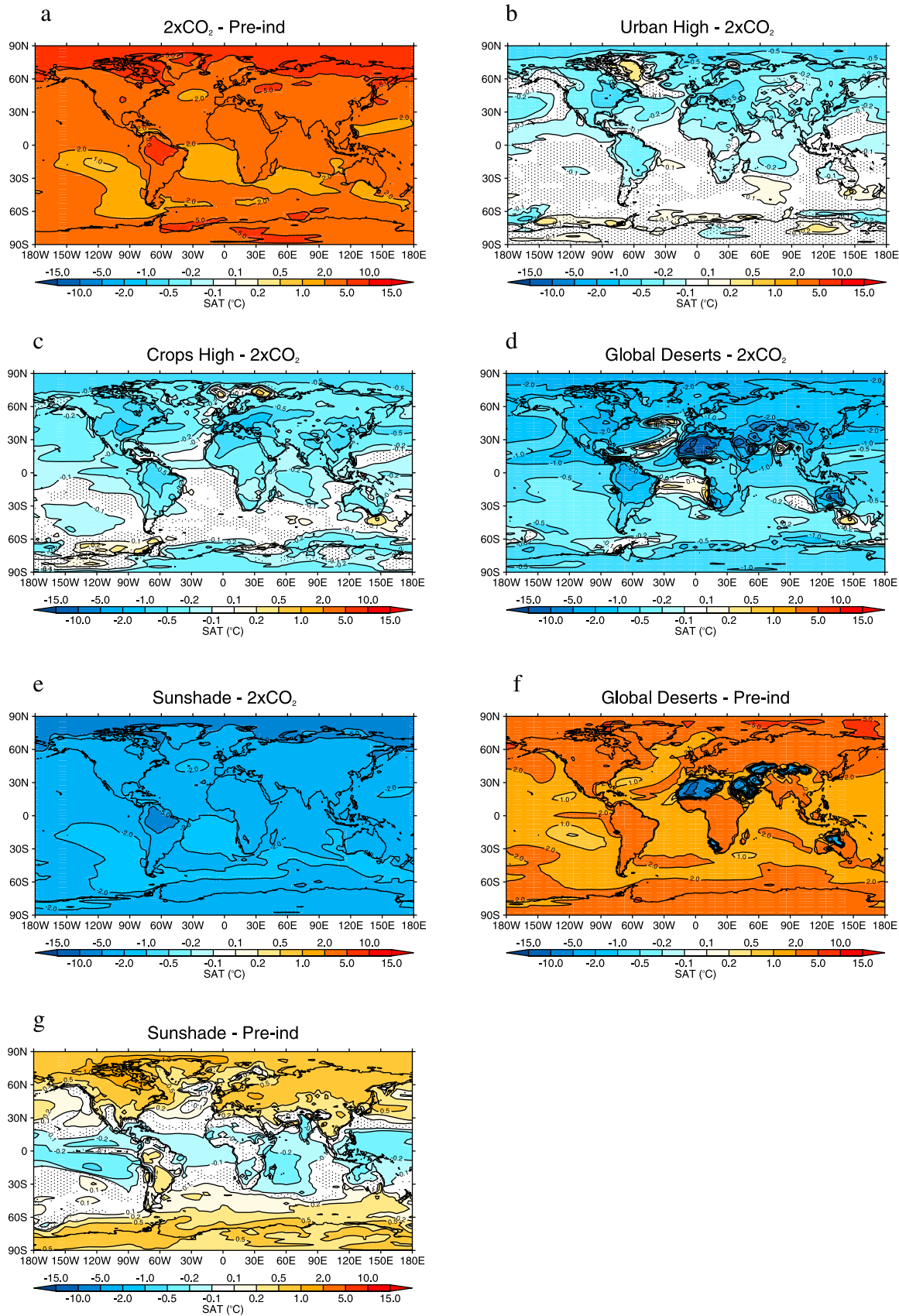


**Figure 2.** This shows the surface air temperature (SAT) anomaly between  $2 \times \text{CO}_2$  and preindustrial and between the various geoengineering schemes and  $2 \times \text{CO}_2$ . Areas that failed a 5% student *t* test are stippled.

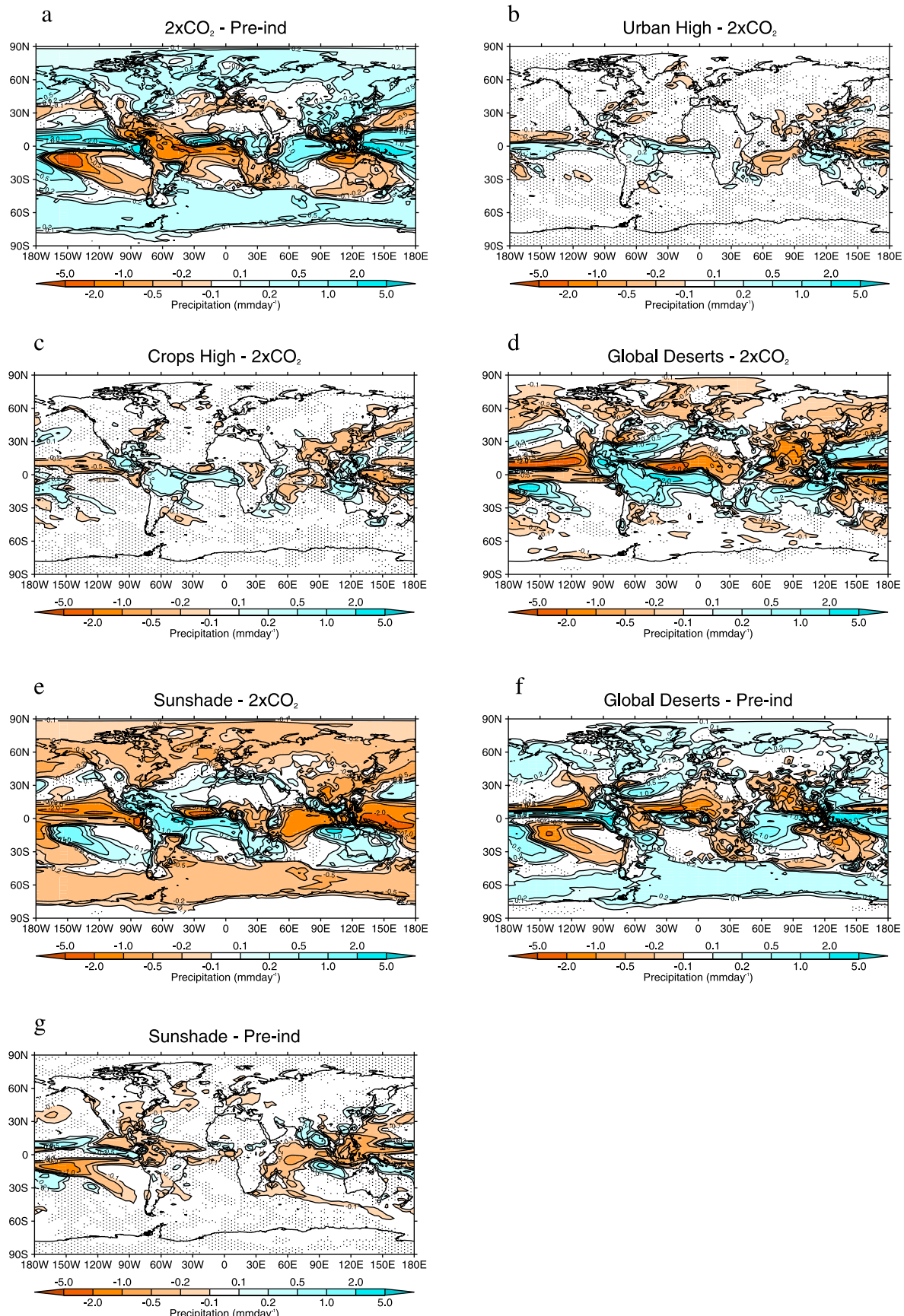


**Figure 3.** This shows the anomaly between  $2 \times \text{CO}_2$  and preindustrial and between the various geoengineering schemes and  $2 \times \text{CO}_2$ . Areas that failed a 5% student *t* test are stippled.

[39] Urban and crop albedo techniques generally induce only small changes in precipitation, with few areas that exhibit a statistically significant change (Figures 3b and 3c). The changes in precipitation that do occur are consistent with a small southward shift of the (Intertropical Convergence Zone (ITCZ), which is induced by an unequal change in the temperature between the Northern and Southern Hemispheres. Both schemes also result in slightly altered precipitation patterns around southeast Asia, the Indian Ocean, and Australasia, changes that are more marked with crop albedo geoengineering than urban. These changes in precipitation are due to changes in evaporation that occur locally and changes in circulation that redistribute rainfall.

[40] Our prescribed enhancement of desert albedo induces shifts in precipitation patterns (Figure 3d) of comparable magnitude to those that arise from doubling CO<sub>2</sub> levels alone (i.e., unmitigated climate change) (Figure 3a). The most prominent changes occur in monsoonal regions such as sub-Saharan Africa, Southeast Asia, and Australia, where the decrease in rainfall leaves these regions drier than in the preindustrial simulation (Figure 3f). Northern South America and Central America experience increases in precipitation that are sufficient to reverse the drying caused by doubling CO<sub>2</sub>.

[41] In comparison, sunshade geoengineering produces a reduction in precipitation in most regions relative to 2 × CO<sub>2</sub>, with some large positive and negative anomalies in the tropics (Figure 3e). When compared with preindustrial areas, few regions experience statistically different precipitation, with exceptions occurring mostly in the tropics (Figure 3g).

[42] The climatology of the HadCM3 model employed here reproduces many of the first-order features of the global climate system but, as with all models, is not perfect, and HadCM3 has some specific deficiencies that should be borne in mind when considering the results presented here:

[43] Although HadCM3 reproduces the global patterns of surface air temperature, it exhibits a cold bias at high latitudes in the Northern Hemisphere, which is particularly pronounced in Russia, east of Scandinavia, and the coarse-resolution orography leads to local and remote biases [Gordon et al., 2000]. The performance for precipitation is generally less good; the observed global patterns are captured, but significant biases exist: The South Pacific Convergence Zone extends farther and in a more easterly direction than observed (the “double ITCZ” problem), there is a strong wet bias around the maritime continent, and there is a dry bias in India and the northern Amazon region [Solomon et al., 2007].

[44] HadCM3, as with other GCMs, also fails to reproduce the temporal structure of observed “para42” precipitation, with simulated precipitation occurring too frequently and at lower intensity than observed.

### 3.2. European Summertime Changes

[45] Europe is a highly urbanized region with significant areas of agricultural land. It is also a region that experiences periodic damaging heat waves, with the 2003 heat wave causing an estimated 70,000 deaths [Robine et al., 2008]. Climate model projections suggest that average European summer temperatures as warm as in 2003 may become the mean state by the end of the 21st century, with significant implications for human health, energy consumption (air

conditioning), and agriculture in the region [Stott et al., 2004]. Thus, Europe is one of the regions that may potentially benefit most from the application of land albedo geoengineering [Singarayer et al., 2009], with the strongest cooling effect tending to be exerted over the summer months, which should ameliorate some of the effects of extremely warm summers. Because of the relatively large fraction of the land occupied by urban areas and cropland, Europe will experience a cooling significantly greater than the global average [e.g., Ridgwell et al., 2009] under these albedo modification schemes.

[46] To examine the effect of SAM geoengineering on the climate of Europe, we examine results for interannual variability in average annual and summer (June, July, and August (JJA)) temperatures across the region of Western Europe (defined as in Figure 4e). Table 3 summarizes the annual and summer temperature anomalies for the different geoengineering schemes for this region. At 2 × CO<sub>2</sub> there is an increase of 4.18°C in the annual temperature across the region, with a larger increase in summer (5.03°C).

[47] Against the greenhouse warming of 2 × CO<sub>2</sub>, urban geoengineering produces a cooling of 0.50°C annually and 0.57°C in summer for maximum deployment. For urban geoengineering there is a larger cooling for the lowest deployment than for a moderate deployment, which is likely a result of internal variability in the model. Crop albedo geoengineering is more effective than urban geoengineering in Europe, with a maximum deployment cooling by 0.83°C annually and 1.26°C in summer. Desert albedo geoengineering, applied globally, exerts a cooling of 1.55°C annually and 1.53°C in summer across the region.

[48] Rather counterintuitively, desert geoengineering restricted to the Sahara has less of a cooling effect in Europe than when it is restricted to Asia, the consequence of large changes in circulation that occur (see Figure 6). Desert geoengineering cools air locally but this air does not simply diffuse from the desert regions; instead, it is advected in a complicated manner by the patterns of circulation, which are also modified by desert geoengineering.

[49] Figure 4 shows how the frequency distribution of summer average temperatures over western Europe is affected by SAM geoengineering. At 2 × CO<sub>2</sub> there is a much warmer summer (~5°C warmer than the preindustrial on average), and during the 100 year period analyzed, all summers were warmer than the warmest preindustrial summer. A number of particularly warm summers also occur; four times with an average temperature above 23°C and once with an average temperature between 24°C and 25°C. High urban geoengineering (Figure 4a) lowers the average summer temperature by ~0.6°C, reducing the number of extremely warm summers. Crop albedo geoengineering (Figure 4b) is more effective, and the greatest intervention lowers average summer temperatures by 1.3°C. With global desert geoengineering (Figure 4c) there is a cooling in the summer of 1.5°C and a reduction in the number of extremely warm summers.

[50] The simulation of European surface air temperature in HadCM3 suffers from a cold bias of around 1°C–2°C in this region. Stott et al. [2004] found that internal variability in European summer temperatures in HadCM3 is similar to observed values, but the model might overestimate variability somewhat (note, however, that the region

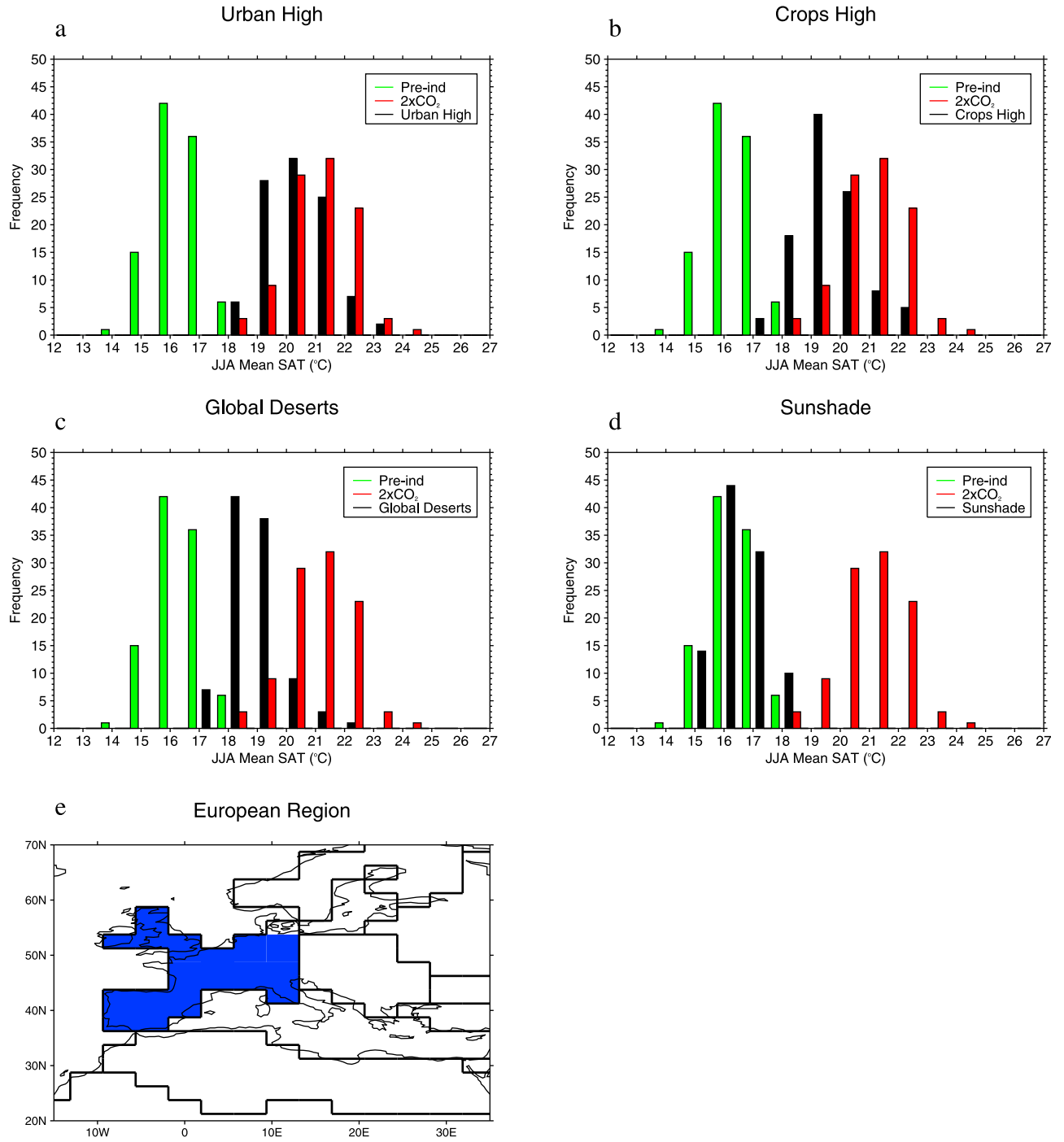


**Figure 4.** Average summer (JJA) surface air temperature in the region in Figure 4e and the frequency with which each temperature occurs over a 100 year period for preindustrial,  $2 \times \text{CO}_2$ , and  $2 \times \text{CO}_2$  with geoengineering. The (a) urban high, (b) crops high, (c) global deserts, and (d) sunshade results are shown.

they defined differs from ours). In simulations of European climate with Regional climate models driven by HadAM3H (a high-resolution atmosphere-only version of HadCM3), it was found that higher resolution orography could improve the spatial patterns of surface air temperature but that problems with land surface schemes and the driving GCM's representation of blocking highs affected the surface air temperature variability [Jacob *et al.*, 2007]. These problems with the land surface schemes and with blocking highs

affect our model and hence our results. However, despite these problems, these results reveal the important local and seasonal effects of these SAM geoengineering schemes.

### 3.3. Monsoon Changes

[51] As was noted earlier, global desert geoengineering may cause large changes in precipitation patterns around the world, particularly in monsoon regions such as India, sub-Saharan Africa, and Australia, because of the mechanism that

**Table 3.** SAT Change in Western Europe<sup>a</sup>

Experiments	SAT (°C)	
	Annual	JJA
2 × CO <sub>2</sub> , Preind	4.18	5.03
Urban High, 2 × CO <sub>2</sub>	-0.50	-0.57
Urban Mid, 2 × CO <sub>2</sub>	-0.14	-0.20
Urban Low, 2 × CO <sub>2</sub>	-0.26	-0.22
Crops High, 2 × CO <sub>2</sub>	-0.83	-1.26
Crops Mid, 2 × CO <sub>2</sub>	-0.49	-0.80
Crops Low, 2 × CO <sub>2</sub>	-0.27	-0.44
Global Deserts, 2 × CO <sub>2</sub>	-1.55	-1.53
Sahara Desert, 2 × CO <sub>2</sub>	-0.74	-0.98
Asian Deserts, 2 × CO <sub>2</sub>	-1.20	-1.49
Sunshade, 2 × CO <sub>2</sub>	-3.47	-4.01

<sup>a</sup>All values passed a 5% student *t* test for statistical significance.

drives monsoon circulations: seasonal land-sea temperature differences. In the normal sequence of events, during the summer months continental areas warm faster than ocean areas, creating a pressure difference: this causes air to circulate, with warm, dry air rising over the continents being replaced by cooler, moist air from the ocean. In winter the opposite occurs as the oceans retain the heat collected over the summer for longer than the land does. With desert geoengineering, there is a large change in albedo of the continental land surface, resulting in cooler summer temperatures, which reduce monsoon circulation locally and lead to significant changes in regional precipitation patterns and also changes in global circulation patterns.

[52] Figure 5a shows the difference between June, July, August (JJA) and December, January, February (DJF) rainfall for the preindustrial. The monsoon systems have a positive difference in precipitation in the north and a negative difference in the south, i.e., greater rainfall in the summer relative to the winter in their respective hemispheres. Figure 5b shows the changes in precipitation seasonality between 2 × CO<sub>2</sub> and preindustrial; there is an intensification of the seasonality of rainfall in Southeast Asia and Indonesia and a reduction in the Amazon region and around the Caribbean. For both urban and crop geoengineering, we find few statistically significant changes in the seasonality of rainfall and so these results are not shown here. For global desert geoengineering, there is a large reduction in monsoonal rains in areas neighboring the modified desert areas (Figures 5c–5e). Global desert geoengineering reduces the intensity of the Indian, East Asian, North African, and Australian monsoons but intensifies seasonal rains in Central and South America relative to 2 × CO<sub>2</sub> (Figure 5c). On the whole there is a large reduction in summer continental rainfall across the tropics compared with that of the preindustrial (Figure 5g).

[53] Restricting desert albedo modification to the Sahara (Figure 5f) reduces the intensity of the North African monsoon and to a lesser extent the Asian monsoon, whereas Asian desert geoengineering (Figure 5g) reduces the intensity of the Asian monsoon and, perhaps surprisingly,

strengthens the North African monsoon, and both schemes increase summer rainfall over Central and South America.

[54] In comparison, sunshade geoengineering reverses most of the effects that doubling CO<sub>2</sub> has on precipitation seasonality (Figure 5f), returning the seasonality of precipitation very close to the preindustrial precipitation, with few statistically significant changes (Figure 5h).

[55] In Figure 6 we show the seasonal changes in 850 hPa winds for global desert geoengineering alongside the changes in precipitation. Desert geoengineering profoundly changes the atmospheric circulation (Figures 6a and 6b), with the most extreme changes occurring in the Northern Hemisphere summer, when the desert albedo changes have their greatest effect (compare Figures 6a and 6b). The altered patterns of precipitation (Figures 6c and 6d) correlate well with changes in 850 hPa wind, i.e., there are changes in moisture advection driven by the changes in the winds. This can be seen, for example, along the Ivory Coast, where a large reduction in JJA rainfall coincides with a seaward wind anomaly (i.e., a reduction in monsoonal, landward winds), and in Central America, where the increase in JJA rainfall coincides with an increase in Pacific to Atlantic winds over the isthmus (Figures 6a and 6c). In Australia, where there are reductions in precipitation, an anticyclonic anomaly in 850 hPa wind during the Austral summer (DJF) acts to reduce the advection of moisture into the north of the continent (Figures 6b and 6d). In general, desert albedo geoengineering leads to a disruption of precipitation locally and remotely through changes in circulation and therefore in moisture advection.

[56] We identify six different areas of interest that may be affected significantly by desert geoengineering (Figure 7g). The percentages of change in average annual precipitation for each of these six regions under different geoengineering scenarios are summarized in Table 4. Brazil experiences a large decrease in precipitation at 2 × CO<sub>2</sub> compared to preindustrial, and all the geoengineering schemes increase precipitation in Brazil, with global desert geoengineering returning precipitation to just above the preindustrial value.

[57] In the two African regions considered there are small increases in precipitation at 2 × CO<sub>2</sub>, and for crop and urban geoengineering there is little effect on average precipitation. Global and Saharan desert geoengineering causes large decreases in precipitation in the Sahel and Ivory Coast regions, whereas Asian desert geoengineering causes a large increase in the Sahel band.

[58] In India and Southeast Asia there are moderate increases in precipitation at 2 × CO<sub>2</sub>; both crops and urban geoengineering reduce rainfall in these regions, particularly in India, although it remains above the preindustrial value. Global desert geoengineering decreases rainfall in India significantly and in Southeast Asia to some extent, with a 37% reduction in rainfall, relative to preindustrial in India, and a 6% decrease in Southeast Asia.

[59] Australia experiences a reduction in precipitation at 2 × CO<sub>2</sub>, and most geoengineering schemes considered increase precipitation in Australia, whereas global desert

**Figure 5.** (a) JJA-DJF precipitation, i.e., the seasonality of precipitation, for the preindustrial. (b–g) Change in seasonality, i.e., the difference in absolute JJA-DJF precipitation, with negative numbers showing a decrease in seasonality. For 2 × CO<sub>2</sub> the anomaly is taken with the preindustrial (Figure 5b), and for the geoengineering schemes the anomaly is taken with the 2 × CO<sub>2</sub> case (Figures 5c–5g). Areas that failed a 5% student *t* test are stippled.

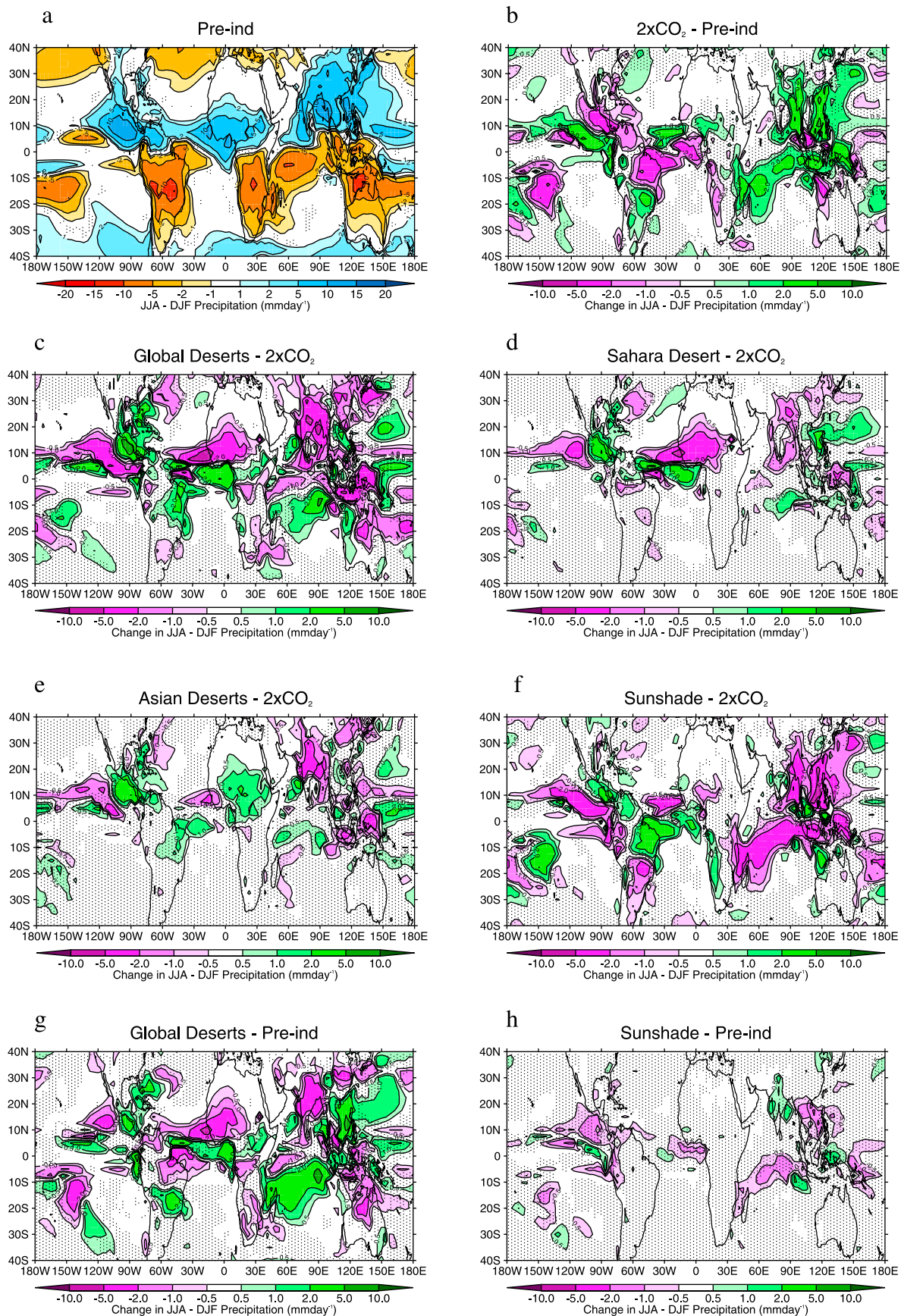
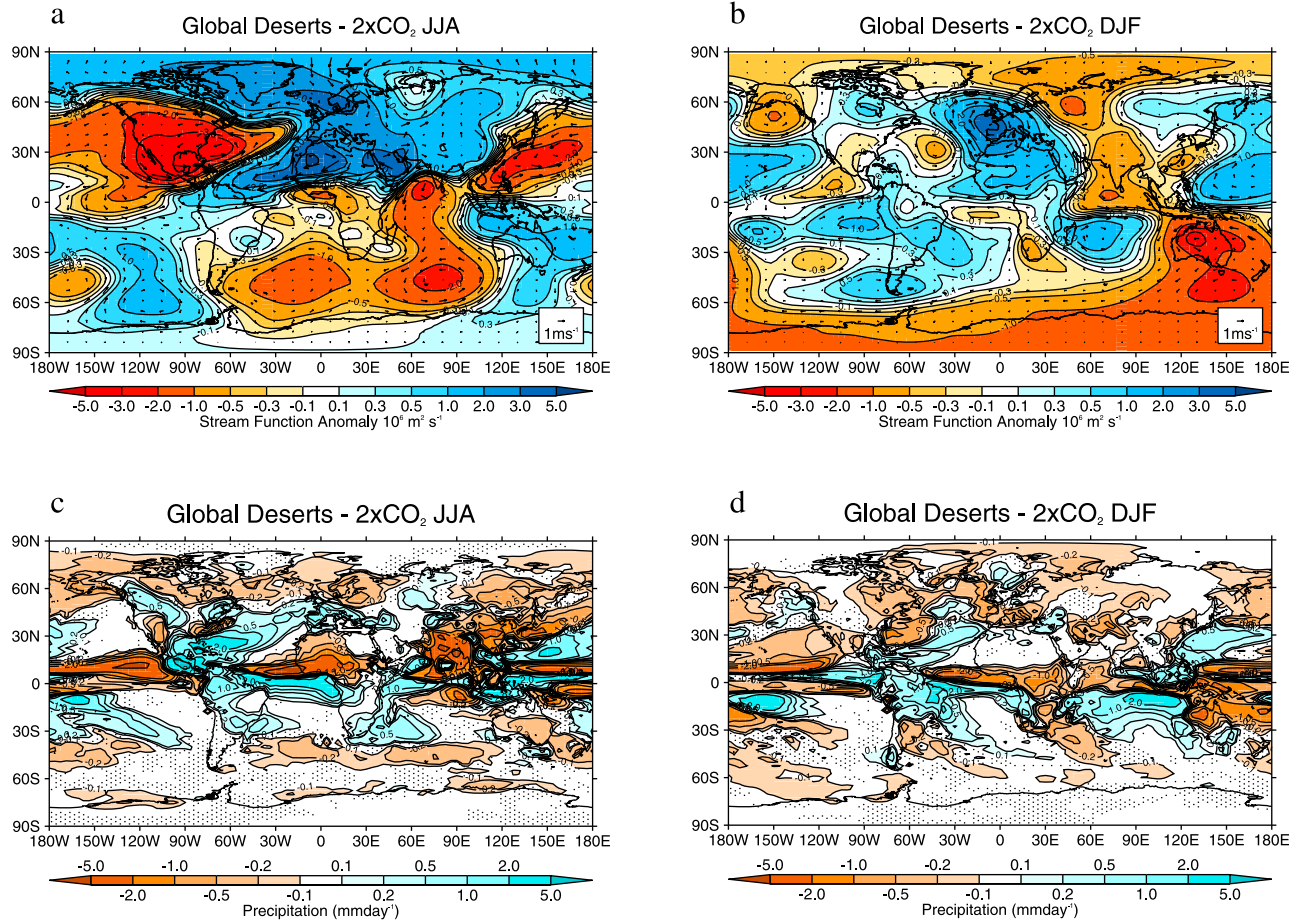


Figure 5



**Figure 6.** This shows the changes between global desert geoengineering and  $2 \times \text{CO}_2$  for the wind speed and stream function at 850 hPa during (a) JJA and (b) DJF and for precipitation during the same periods (Figures 6c and 6d), respectively. For precipitation, areas that failed a 5% student *t* test are stippled.

geoengineering (which includes an Australian component) produces an 18% reduction in rainfall compared with the preindustrial.

[60] Variability in monsoon rainfall is also an important indicator of change; Figure 7 shows frequency plots for annual precipitation over India (in Figure 7g the Indian region is shaded blue). The rainfall distribution changes from preindustrial to  $2 \times \text{CO}_2$  with average rainfall up 15% and fewer dry years. Figure 7a shows that urban geoengineering reduces the rainfall over India slightly, returning the distribution somewhat closer to its preindustrial state. Crop geoengineering has a larger impact, returning the mean rainfall over India close to preindustrial values but broadening the distribution (Figure 7b).

[61] The desert geoengineering schemes applied globally, in the Sahara, and in Asia, all reduce Indian rainfall, resulting in a 37% reduction, no statistically significant change, and an 18% reduction relative to the preindustrial, respectively (Figures 7c–7e). For global desert geoengineering the

wettest years are below the preindustrial mean and, in the driest years, India receives less than 300 mm of rain, down from more than 500 mm in the preindustrial. Asian desert geoengineering has a significant drying effect, whereas Sahara desert geoengineering returns the distribution close to that of the preindustrial state.

[62] *Dabang et al. [2005]* assessed some of the models used in the Coupled Model Intercomparison Project 3 (CMIP3) for their performance in reproducing the East Asian monsoon and found that all models had difficulties reproducing the observed behavior but that HadCM3 was one of the better models. They found that while HadCM3 overestimated precipitation in all seasons, the distribution of precipitation was similar to that of observations, and although the winter was too cold, the surface air temperature was well reproduced. These problems and others affect the quality of the monsoon results shown, and so the details of the results must be viewed with caution. However, because of desert geoengineering directly affecting the seasonal

**Figure 7.** Average annual precipitation in India (see Figure 7g) and the frequency with which the volumes of precipitation occur over a 100 year period for preindustrial,  $2 \times \text{CO}_2$ , and  $2 \times \text{CO}_2$  with geoengineering. The (a) urban high, (b) crops high, (c) global, (d) Asian deserts, (e) Sahara deserts, and (f) sunshade results are shown. Figure 7g shows the regions that were used to calculate the area-averaged changes in precipitation; these are based on the regions in the FUND model [*Anthoff et al., 2009*].

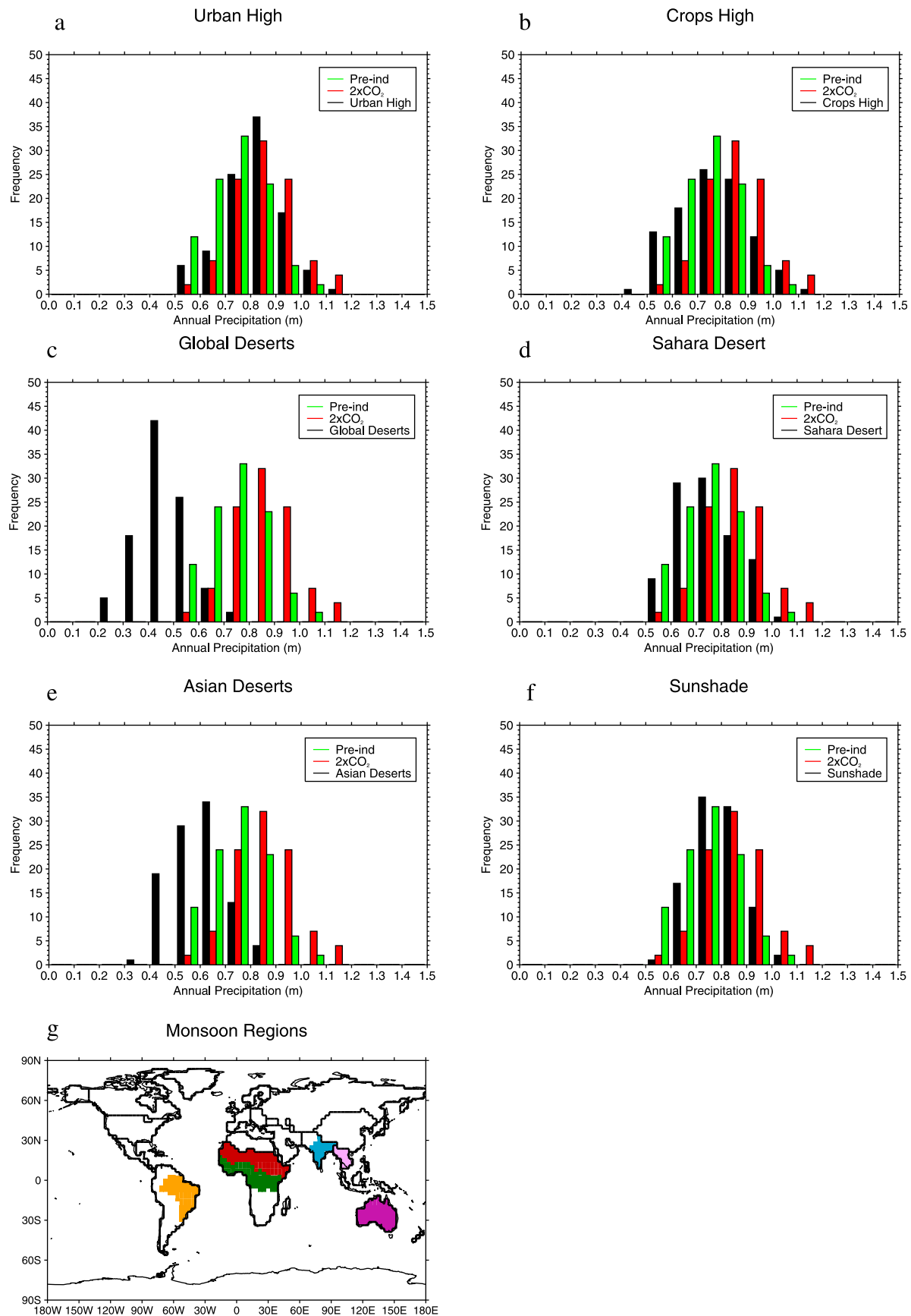


Figure 7

**Table 4.** Precipitation Change in Monsoon Regions<sup>a</sup>

Experiments	Precipitation Change (%)					
	Brazil	Sahel	Ivory Coast	India	SE Asia	Australia
2 × CO <sub>2</sub> , Preind	<b>-21.7</b>	<b>5.2</b>	<b>6.6</b>	<b>14.8</b>	<b>7.5</b>	<b>-14.3</b>
Urban High, 2 × CO <sub>2</sub>	<b>4.6</b>	0.7	-0.2	<b>-3.8</b>	-1.7	4.7
Crops High, 2 × CO <sub>2</sub>	<b>6.8</b>	0.5	-0.4	<b>-9.8</b>	<b>-2.3</b>	2.3
Global Deserts, 2 × CO <sub>2</sub>	<b>28.8</b>	<b>-30.6</b>	<b>-17.4</b>	<b>-45.0</b>	<b>-12.8</b>	<b>-18.2</b>
Sahara Desert, 2 × CO <sub>2</sub>	<b>10.8</b>	<b>-33.4</b>	<b>-19.1</b>	<b>-12.5</b>	<b>-4.8</b>	-2.8
Asian Deserts, 2 × CO <sub>2</sub>	<b>10.5</b>	<b>19.0</b>	<b>2.0</b>	<b>-28.7</b>	<b>-5.0</b>	<b>8.7</b>
Sunshade, 2 × CO <sub>2</sub>	<b>24.9</b>	<b>-5.1</b>	<b>-5.7</b>	<b>-6.6</b>	<b>-10.3</b>	<b>17.7</b>

<sup>a</sup>Boldface values passed a 5% student *t* test for statistical significance.

land-sea temperature difference, the driver of monsoon circulation, the general result of reduced rainfall near modified desert regions is likely to be robust.

### 3.4. Arctic Changes

[63] The Arctic is a region that is warming faster than the rest of the world, as a result of global warming [IPCC, 2007]. Although the exact mechanisms are uncertain, retreating sea ice and, to a lesser extent, changes in snow cover are likely to be involved [Screen and Simmonds, 2010]. The Arctic is home to large reservoirs of stored carbon, as decayed plant matter in permafrost and methane reserves in hydrates, which could provide an additional (carbon cycle) positive feedback [Archer, 2007]. We focus on the Arctic here for these reasons as well as the fact that it is remote from all the SAM schemes and hence illustrates the potential for nonlocal impacts (and teleconnections) arising from land albedo geoengineering.

[64] Figure 8 shows the simulated preindustrial sea-ice and snow coverage for the Northern Hemisphere and the effects of doubling CO<sub>2</sub> and geoengineering on sea ice and snow. Comparing Figures 8a and 8b, it can be seen that the sea-ice extent and thickness are reduced at 2 × CO<sub>2</sub> compared to preindustrial, with minimum sea-ice cover (September average) reduced by 71% (Figure 8c). The change in snow depth is more spatially heterogeneous, with snow loss at midlatitudes but an increase in snow depth at high latitudes. At high latitudes the increase in snow accumulation outweighs the increased losses that are due to higher temperatures, and with a greater fraction of the Arctic Ocean ice free there will be more evaporation and consequently greater snowfall (the increase in precipitation is shown in Figure 3a). The snow depth projections for Greenland are omitted as the model does not include an ice sheet module and so cannot simulate changes in this region reasonably.

[65] Figures 8c and 8d show that urban and cropland geoengineering induce a slight recovery of annual mean sea-ice thickness, with 13% and 20% increases, respectively, in minimum sea-ice cover (September average) relative to 2 × CO<sub>2</sub> and a very small effect on snow depth. Desert geoengineering exerts a more substantial effect on

annual mean sea-ice thickness, with a 65% increase in minimum sea-ice cover relative to 2 × CO<sub>2</sub>, which remains 53% lower than the preindustrial coverage. Desert geoengineering also has a large impact on snow depth, with almost the opposite spatial pattern to that of 2 × CO<sub>2</sub>; i.e., desert geoengineering cools and dries the Northern Hemisphere, partly reversing the trend induced by global warming.

[66] Again, projections of effects of geoengineering on climate must be viewed in the context of the degree of fidelity of the climate model used: HadCM3 has a number of biases in the climate state of high northern latitudes that will affect the results shown in this section, the most important of which is a cold bias [Gregory et al., 2002]. HadCM3 also has a wet bias at high latitudes that will affect the quality of the snow cover results [Solomon et al., 2007]. There are problems in the sea-ice climatology of HadCM3 but the model does roughly reproduce the 20th-century trend in sea ice [Gregory et al., 2002] and matches the projections of other AOGCMs, predicting a large decline in summer sea-ice extent over the course of the 21st century [Johannessen et al., 2004]. However, the results shown are consistent with the cooling of the SAM schemes being concentrated in the Northern Hemisphere and show that SAM geoengineering may help to reduce Arctic climate change somewhat.

## 4. Discussion and Conclusion

[67] Global average measures of climate change alone are insufficient in the assessment of the effectiveness and, particularly, side effects of surface albedo geoengineering. Analyses of regional and seasonal changes in temperature, precipitation, and other variables are critical to elucidating whether any particular proposed geoengineering scheme may be a suitable means to ameliorate climate change. In this study we have used a fully coupled general circulation model (GCM) to project the climatic effects of different surface albedo modification (SAM) geoengineering schemes. However, GCMs are far from perfect representations of the Earth's climate, and, although they perform relatively well on the large scale, they do not match observations well on small spatial and temporal scales [IPCC, 2007]. GCMs are particularly poor at reproducing regional precipitation observations, and so any specific patterns of precipitation change should be viewed with caution [IPCC, 2007]. In addition to these considerations, and as well as deficiencies specific to the HadCM3 model discussed in earlier sections, the MOSES 1 land surface scheme we use assumes fixed vegetation and so does not allow adjustments to changed climatological conditions. Vegetation feedbacks will hence not be captured in our simulations.

[68] Our treatment of surface albedo geoengineering is relatively simplistic, and there are no explicit urban, cropland, or desert surface land types in the MOSES 1 land surface scheme [Cox et al., 1999] we employ here. Areas to which we applied surface albedo geoengineering could also have been alternatively defined. For instance, our definition

**Figure 8.** (a and b) Preindustrial and 2 × CO<sub>2</sub> simulated snow and sea ice cover. (c) The difference in snow and sea-ice cover between 2 × CO<sub>2</sub> and preindustrial. (d–g) Difference between the geoengineering experiments and 2 × CO<sub>2</sub>. Urban high geoengineering (Figure 8c), crops high geoengineering (Figure 8d), global desert geoengineering (Figure 8e), and sunshade geoengineering (Figure 8f). The results for Greenland have been masked out as the model does not include a representation of ice sheet processes. Areas that fail a 5% student *t* test are stippled.

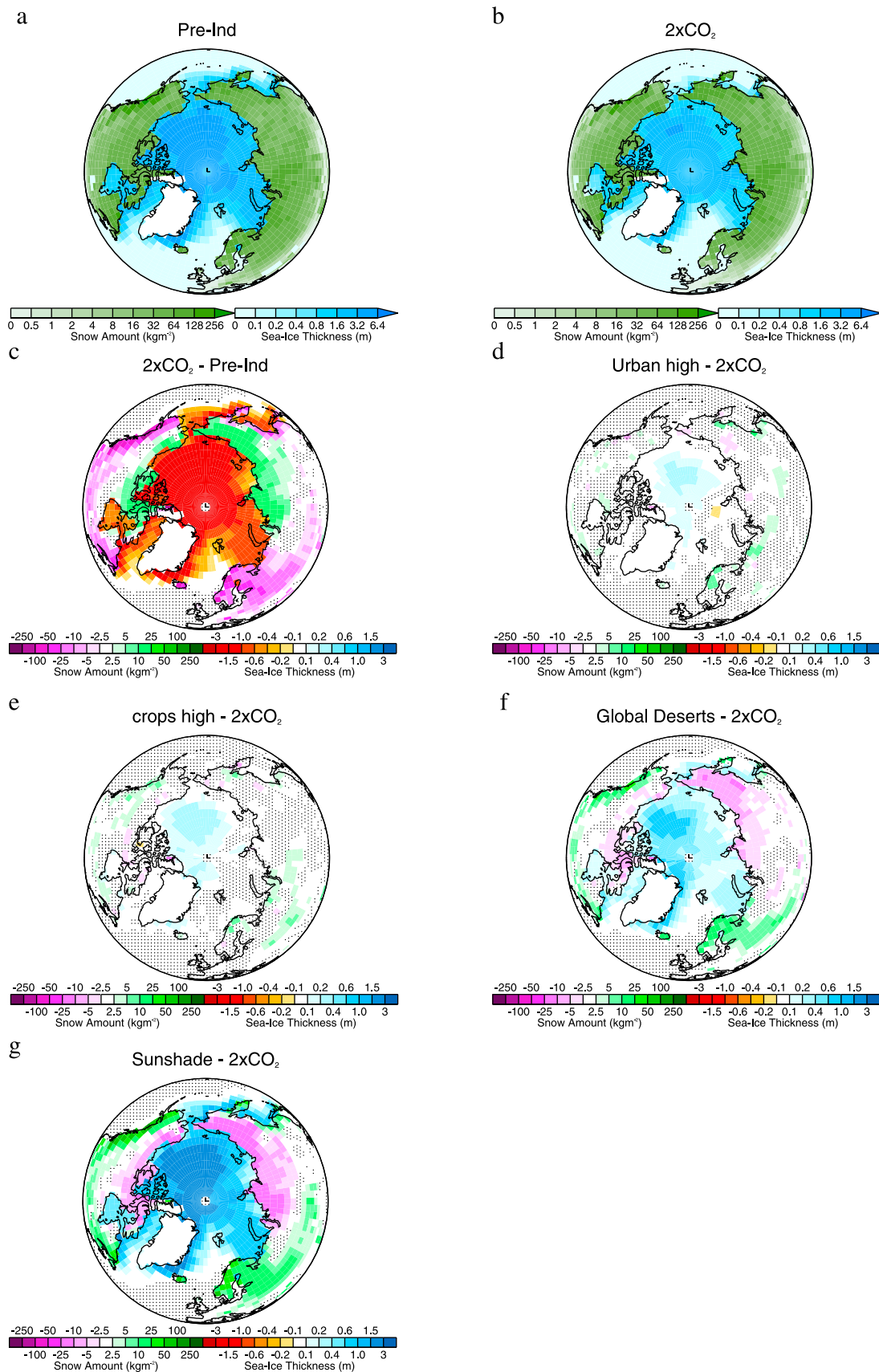


Figure 8

of desert was based on grid-scale-sized areas, excluding smaller deserts, and hence our distribution of desert geoengineering could be revised. Given the extreme nature of desert albedo modification, a different distribution of modified desert would likely produce a significantly different regional response, which can be seen by comparing the very different responses from our three different areas of application. The assumed magnitudes of geoengineering we deployed for each scheme and in particular for urban geoengineering are generally at the upper end of estimates and do not necessarily represent “realistic” scenarios. We chose to mostly test relatively large-magnitude albedo modifications in order to obtain a sufficient signal-to-noise ratio and thus to enable us to more fully explore the potential climatic consequences of highly concentrated changes in albedo. Overall, however, we believe the distributions we used capture the essential properties of these schemes, and at a minimum our study provides a unique sensitivity test for the climate impacts of the three main proposals for surface albedo geoengineering.

[69] Surface albedo modification (SAM) geoengineering gives rise to both near-field and far-field changes in climate. We find small to insignificant changes in global average temperatures from urban and crop geoengineering, consistent with other studies [Lenton and Vaughan, 2009; Ridgwell et al., 2009], and a more significant cooling with desert geoengineering. For all the SAM schemes we find a local cooling around the region with modified albedo, which is greatest in summer, although we found this effect can be reduced somewhat by changes in cloud feedbacks and advection, as has been found in other studies of SAM geoengineering [Doughty et al., 2011; Ridgwell et al., 2009].

[70] On a global scale we find that the cooling effect of the SAM geoengineering schemes is greater over land and in the Northern Hemisphere because of the greater fraction of suitable regions being in the Northern Hemisphere. We find that the Arctic is cooled somewhat by all schemes, despite being remote from any areas of application, and there is some recovery of sea ice and snow cover, but even desert geoengineering is insufficient to return the Arctic sea ice and snow to their preindustrial conditions.

[71] We find that very large changes in precipitation patterns can occur for desert geoengineering, with much smaller changes for urban and crop geoengineering. We compared desert geoengineering with sunshade geoengineering and with the results of a cloud albedo study and found that although desert geoengineering produces a smaller reduction in global average precipitation per change in temperature, it causes a much greater reduction in the land-average precipitation [Bala et al., 2010]. This is consistent with, but opposite to, the results found in the cloud albedo study of Bala et al. [2010], in which they found a large reduction in global average precipitation but a much smaller reduction in land-average precipitation. This is explained in their study by the warmer region (the land in their case or ocean in ours) having an increase in upward motion in the atmosphere, giving rise to increased precipitation, with the opposite being true for the colder region [Bala et al., 2010]. Similarly we find for urban and crop geoengineering that the relative cooling of the Northern Hemisphere leads to a slight southward shift of the ITCZ that for desert geoengineering is hard

to distinguish because of the dramatic changes in circulation arising from the extreme local cooling.

[72] Desert geoengineering causes large changes to continental rainfall in regions neighboring deserts and more broadly causes significant changes in tropical rainfall patterns. These changes arise, in part, because of the seasonal nature of the cooling exerted by SAM geoengineering, with the greatest cooling occurring in summer, when the air over the continents would normally warm faster than the ocean, creating an updraft, which draws in moist air from the oceans bringing seasonal rainfall. This monsoon circulation is reduced by desert geoengineering, leading to a reduction in precipitation across a wide area. We find that precipitation across the tropics is radically shifted, with some areas becoming much drier than in the preindustrial, particularly India, and others becoming wetter.

[73] SAM geoengineering schemes do not offer anything like a full solution to the problems arising from rising greenhouse gas concentrations, and desert geoengineering, in particular, may prove to be detrimental. Our simulations show that urban and crop geoengineering may have little effect on global climates and primarily offer only local ameliorations of some climate change effects. Desert geoengineering, on the other hand, produces strong local cooling in desert regions and results in large changes in circulation and precipitation worldwide. Not only are land albedo geoengineering schemes unable to correct fully for greenhouse-gas-induced climate changes (as is the case for all SRM schemes investigated so far [e.g., Lunt et al., 2008; Irvine et al., 2010; Jones et al., 2011; Ban-Weiss and Caldeira, 2010]), they would not address ocean acidification [Cao and Caldeira, 2008; Matthews et al., 2009]. Only mitigation of CO<sub>2</sub> emissions or removal of CO<sub>2</sub> from the atmosphere by some carbon dioxide removal scheme [Shepherd et al., 2009] would provide a correction for both the climatic and ocean chemistry impacts of elevated CO<sub>2</sub> concentrations. Future work on SAM geoengineering could look in more detail at the impacts of these schemes with a higher-resolution GCM or a regional climate model or consider combinations of surface albedo modification and other climate engineering schemes as a way to “optimize” the climate modification.

[74] **Acknowledgments.** P.I. is funded on a NERC Ph.D. studentship. A.R. acknowledges support from the Royal Society in the form of a university research fellowship. D.L. acknowledges funding from the RCUK in the form of a research fellowship. A.R. also acknowledges EPSRC grant EP/I014721/1.

## References

- Akbari, H., S. Menon, and A. Rosenfeld (2009), Global cooling: Increasing world-wide urban albedos to offset CO<sub>2</sub>, *Clim. Change*, 94(3–4), 275–286, doi:10.1007/s10584-008-9515-9.
- Andrews, T., P. M. Forster, O. Boucher, N. Bellouin, and A. Jones (2010), Precipitation, radiative forcing and global temperature change, *Geophys. Res. Lett.*, 37, L14701, doi:10.1029/2010GL043991.
- Angel, R. (2006), Feasibility of cooling the Earth with a cloud of small spacecraft near the inner Lagrange point (L1), *Proc. Natl. Acad. Sci. U. S. A.*, 103(46), 17,184–17,189, doi:10.1073/pnas.0608163103.
- Anthoff, D., C. Hepburn, and R. S. J. Tol (2009), Equity weighting and the marginal damage costs of climate change, *Ecol. Econ.*, 68(3), 836–849, doi:10.1016/j.ecolecon.2008.06.017.
- Archer, D. (2007), Methane hydrate stability and anthropogenic climate change, *Biogeosciences*, 4(4), 521–544, doi:10.5194/bg-4-521-2007.

- Bala, G., K. Caldeira, R. Nemani, L. Cao, G. Ban-Weiss, and H.-J. Shin (2010), Albedo enhancement of marine clouds to counteract global warming: Impacts on the hydrological cycle, *Clim. Dyn.*, 6, 1–17.
- Ban-Weiss, G. A., and K. Caldeira (2010), Geoengineering as an optimization problem, *Environ. Res. Lett.*, 5(3), 034009, doi:10.1088/1748-9326/5/3/034009.
- Betts, R. A., P. D. Falloon, K. K. Goldewijk, and N. Ramankutty (2007), Biogeophysical effects of land use on climate: Model simulations of radiative forcing and large-scale temperature change, *Agric. For. Meteorol.*, 142(2–4), 216–233, doi:10.1016/j.agrformet.2006.08.021.
- Bretz, S., H. Akbari, and A. Rosenfeld (1998), Practical issues for using solar-reflective materials to mitigate urban heat islands, *Atmos. Environ.*, 32(1), 95–101, doi:10.1016/S1352-2310(97)00182-9.
- Caldeira, K., and L. Wood (2008), Global and Arctic climate engineering: Numerical model studies, *Philos. Trans. R. Soc. A*, 366(1882), 4039–4056.
- Cao, L., and K. Caldeira (2008), Atmospheric CO<sub>2</sub> stabilization and ocean acidification, *Geophys. Res. Lett.*, 35, L19609, doi:10.1029/2008GL035072.
- Cattle, H., and J. Crossley (1995), Modeling Arctic climate-change, *Philos. Trans. R. Soc. A*, 352(1699), 201–213.
- Collins, W. J., et al. (2011), Development and evaluation of an Earth-system model—HadGEM2, *Geosci. Model Dev. Discuss.*, 4(2), 997–1062, doi:10.5194/gmdd-4-997-2011.
- Commission of European Communities (2007), Limiting global climate change to 2 degrees Celsius: The way ahead for 2020 and beyond, *Pap. 52007DC0002*, 13 pp., Comm. of European Communities, Brussels.
- Costa, M. H., S. N. M. Yanagi, P. Souza, A. Ribeiro, and E. J. P. Rocha (2007), Climate change in Amazonia caused by soybean cropland expansion, as compared to caused by pastureland expansion, *Geophys. Res. Lett.*, 34, L07706, doi:10.1029/2007GL029271.
- Covey, C., K. M. AchutaRao, U. Cubasch, P. Jones, S. J. Lambert, M. E. Mann, T. J. Phillips, and K. E. Taylor (2003), An overview of results from the Coupled Model Intercomparison Project, *Global Planet. Change*, 37(1–2), 103–133, doi:10.1016/S0921-8181(02)00193-5.
- Cox, P. M., R. A. Betts, C. B. Bunton, R. L. H. Essery, P. R. Rowntree, and J. Smith (1999), The impact of new land surface physics on the GCM simulation of climate and climate sensitivity, *Clim. Dyn.*, 15(3), 183–203, doi:10.1007/s003820050276.
- Cox, P. M., R. A. Betts, C. D. Jones, S. A. Spall, and I. J. Totterdell (2000), Acceleration of global warming due to carbon-cycle feedbacks in a coupled climate model, *Nature*, 408(6809), 184–187, doi:10.1038/35041539.
- Crutzen, P. J. (2006), Albedo enhancement by stratospheric sulfur injections: A contribution to resolve a policy dilemma?, *Clim. Change*, 77(3–4), 211–220, doi:10.1007/s10584-006-9101-y.
- Dabang, J., H. J. Wang, and X. M. Lang (2005), Evaluation of east Asian climatology as simulated by seven coupled models, *Adv. Atmos. Sci.*, 22(4), 479–495, doi:10.1007/BF02918482.
- Doughty, C., C. Field, and A. McMillan (2011), Can crop albedo be increased through the modification of leaf trichomes, and could this cool regional climate?, *Clim. Change*, 104(2), 379–387, doi:10.1007/s10584-010-9936-0.
- Essery, R. L. H., M. J. Best, R. A. Betts, P. M. Cox, and C. M. Taylor (2003), Explicit representation of subgrid heterogeneity in a GCM land surface scheme, *J. Hydrometeorol.*, 4(3), 530–543, doi:10.1175/1525-7541(2003)004<0530:EROSHI>2.0.CO;2.
- Febrero, A., S. Fernandez, J. L. Molina-Cano, and J. L. Araus (1998), Yield, carbon isotope discrimination, canopy reflectance and cuticular conductance of barley isolines of differing glaucousness, *J. Exp. Bot.*, 49(326), 1575–1581, doi:10.1093/jexbot/49.326.1575.
- Friedlingstein, P., R. A. Houghton, G. Marland, J. Hackler, T. A. Boden, T. J. Conway, J. G. Canadell, M. R. Raupach, P. Ciais, and C. Le Quere (2010), Update on CO<sub>2</sub> emissions, *Nat. Geosci.*, 3(12), 811–812, doi:10.1038/ngeo1022.
- Gaskill, A. (2004), Summary of meeting with US DOE to discuss geoengineering options to prevent long-term climate change, *Environ. Ref. Mater.*, Inc., Research Triangle Park, N. C.
- Gent, P. R., and J. C. McWilliams (1990), Isopycnal mixing in ocean circulation models, *J. Phys. Oceanogr.*, 20(1), 150–155, doi:10.1175/1520-0485(1990)020<0150:IMOCM>2.0.CO;2.
- Gordon, C., C. Cooper, C. A. Senior, H. Banks, J. M. Gregory, T. C. Johns, J. F. B. Mitchell, and R. A. Wood (2000), The simulation of SST, sea ice extents and ocean heat transports in a version of the Hadley Centre coupled model without flux adjustments, *Clim. Dyn.*, 16(2–3), 147–168, doi:10.1007/s003820050010.
- Grant, R. H., G. M. Heisler, W. Gao, and M. Jenks (2003), Ultraviolet leaf reflectance of common urban trees and the prediction of reflectance from leaf surface characteristics, *Agric. For. Meteorol.*, 120(1–4), 127–139, doi:10.1016/j.agrformet.2003.08.025.
- Gregory, D., and P. R. Rowntree (1990), A mass flux convection scheme with representation of cloud ensemble characteristics and stability-dependent closure, *Mon. Weather Rev.*, 118(7), 1483–1506, doi:10.1175/1520-0493(1990)118<1483:AMFCSW>2.0.CO;2.
- Gregory, J. M., P. A. Stott, D. J. Cresswell, N. A. Rayner, C. Gordon, and D. M. H. Sexton (2002), Recent and future changes in Arctic sea ice simulated by the HadCM3 AOGCM, *Geophys. Res. Lett.*, 29(24), 2175, doi:10.1029/2001GL014575.
- Global Rural-Urban Mapping Project (GRUMP) (2005), Gridded Population of the World and the Global Rural-Urban Mapping Project Data Set, <http://sedac.ciesin.columbia.edu/gpw/>, Socioecon. Data and Appl. Cent., Palisades, N. Y.
- Hamwey, R. (2007), Active amplification of the terrestrial albedo to mitigate climate change: An exploratory study, *Mitig. Adapt. Strategies Glob. Change*, 12(4), 419–439, doi:10.1007/s11027-005-9024-3.
- Hansen, M. C., R. S. Defries, J. R. G. Townshend, and R. Sohlberg (2000), Global land cover classification at 1 km spatial resolution using a classification tree approach, *Int. J. Remote Sens.*, 21(6–7), 1331–1364, doi:10.1080/014311600210209.
- Hatfield, J. L., and R. E. Carlson (1979), Light quality distributions and spectral albedo of three maize canopies, *Agric. Meteorol.*, 20(3), 215–226, doi:10.1016/0002-1571(79)90022-0.
- Holmes, M. G., and D. R. Keiller (2002), Effects of pubescence and waxes on the reflectance of leaves in the ultraviolet and photosynthetic wavebands: A comparison of a range of species, *Plant Cell Environ.*, 25(1), 85–93, doi:10.1046/j.1365-3040.2002.00779.x.
- Intergovernmental Panel on Climate Change (IPCC) (2007), *Climate Change 2007: The Physical Science Basis: Contribution of Working Group I to the Fourth Assessment Report of the Intergovernmental Panel on Climate Change*, edited by D. Q. S. Solomon et al., 996 pp., Cambridge Univ. Press, Cambridge, U. K.
- Irvine, P. J., D. J. Lunt, E. J. Stone, and A. Ridgwell (2009), The fate of the Greenland Ice Sheet in a geoengineered, high CO<sub>2</sub> world, *Environ. Res. Lett.*, 4(4), 045109, doi:10.1088/1748-9326/4/4/045109.
- Irvine, P. J., A. Ridgwell, and D. J. Lunt (2010), Assessing the regional disparities in geoengineering impacts, *Geophys. Res. Lett.*, 37, L18702, doi:10.1029/2010GL044447.
- Jacob, D., et al. (2007), An inter-comparison of regional climate models for Europe: Model performance in present-day climate, *Clim. Change*, 81, 31–52, doi:10.1007/s10584-006-9213-4.
- Johannessen, O. M., et al. (2004), Arctic climate change: Observed and modelled temperature and sea-ice variability, *Tellus Ser. A*, 56(4), 328–341.
- Johns, T. C., et al. (2003), Anthropogenic climate change for 1860 to 2100 simulated with the HadCM3 model under updated emissions scenarios, *Clim. Dyn.*, 20(6), 583–612.
- Jones, A., J. Haywood, and O. Boucher (2011), A comparison of the climate impacts of geoengineering by stratospheric SO<sub>2</sub> injection and by brightening of marine stratocumulus cloud, *Atmos. Sci. Lett.*, 12(2), 176–183, doi:10.1002/asl.291.
- Lambert, F. H., and M. J. Webb (2008), Dependency of global mean precipitation on surface temperature, *Geophys. Res. Lett.*, 35, L16706, doi:10.1029/2008GL034838.
- Le Quéré, C., et al. (2009), Trends in the sources and sinks of carbon dioxide, *Nat. Geosci.*, 2(12), 831–836, doi:10.1038/ngeo689.
- Lenton, T. M., and N. E. Vaughan (2009), The radiative forcing potential of different climate geoengineering options, *Atmos. Chem. Phys.*, 9(15), 5539–5561, doi:10.5194/acp-9-5539-2009.
- Loveland, T. R., B. C. Reed, J. F. Brown, D. O. Ohlen, Z. Zhu, L. Yang, and J. W. Merchant (2000), Development of a global land cover characteristics database and IGBP DISCover from 1 km AVHRR data, *Int. J. Remote Sens.*, 21(6–7), 1303–1330, doi:10.1080/014311600210191.
- Lunt, D. J., A. Ridgwell, P. J. Valdes, and A. Seale (2008), “Sunshade World”: A fully coupled GCM evaluation of the climatic impacts of geoengineering, *Geophys. Res. Lett.*, 35, L12710, doi:10.1029/2008GL033674.
- Martin, G. M., M. A. Ringer, V. D. Pope, A. Jones, C. Dearden, and T. J. Hinton (2006), The physical properties of the atmosphere in the new Hadley Centre Global Environmental Model (HadGEM1). Part I: Model description and global climatology, *J. Clim.*, 19(7), 1274–1301, doi:10.1175/JCLI3636.1.
- Matthews, H. D., A. J. Weaver, M. Eby, and K. J. Meissner (2003), Radiative forcing of climate by historical land cover change, *Geophys. Res. Lett.*, 30(2), 1055, doi:10.1029/2002GL016098.
- Matthews, H. D., L. Cao, and K. Caldeira (2009), Sensitivity of ocean acidification to geoengineered climate stabilization, *Geophys. Res. Lett.*, 36, L10706, doi:10.1029/2009GL037488.
- Monteith, J. L., and M. H. Unsworth (1990), *Principles of Environmental Physics*, 2nd ed., 291 pp., Routledge, London.
- Oleson, K. W., G. B. Bonan, and J. Feddema (2010), Effects of white roofs on urban temperature in a global climate model, *Geophys. Res. Lett.*, 37, L03701, doi:10.1029/2009GL042194.

- Pomerantz, M., H. Akbari, P. Berdahl, S. J. Konopacki, H. Taha, and A. H. Rosenfeld (1999), Reflective surfaces for cooler buildings and cities, *Philos. Mag. B*, 79(9), 1457–1476.
- Ridgwell, A., J. S. Singarayer, A. M. Hetherington, and P. J. Valdes (2009), Tackling regional climate change by leaf albedo bio-geoengineering, *Curr. Biol.*, 19(2), 146–150, doi:10.1016/j.cub.2008.12.025.
- Robine, J.-M., S. L. K. Cheung, S. Le Roy, H. Van Oyen, C. Griffiths, J.-P. Michel, and F. R. Herrmann (2008), Death toll exceeded 70,000 in Europe during the summer of 2003, *C. R. Biol.*, 331(2), 171–178, doi:10.1016/j.crvi.2007.12.001.
- Robock, A., L. Oman, and G. L. Stenchikov (2008), Regional climate responses to geoengineering with tropical and Arctic SO<sub>2</sub> injections, *J. Geophys. Res.*, 113, D16101, doi:10.1029/2008JD010050.
- Salter, S., G. Sortino, and J. Latham (2008), Sea-going hardware for the cloud albedo method of reversing global warming, *Philos. Trans. R. Soc. A*, 366(1882), 3989–4006.
- Screen, J. A., and I. Simmonds (2010), The central role of diminishing sea ice in recent Arctic temperature amplification, *Nature*, 464(7293), 1334–1337, doi:10.1038/nature09051.
- Shepherd, J., et al. (2009), *Geoengineering the Climate: Science, Governance and Uncertainty, RS Policy Doc. 10/09*, Royal Soc., London.
- Singarayer, J. S., A. Ridgwell, and P. Irvine (2009), Assessing the benefits of crop albedo bio-geoengineering, *Environ. Res. Lett.*, 4(4), 045110, doi:10.1088/1748-9326/4/4/045110.
- Smith, R. N. B. (1993), Experience and developments with the layer cloud and boundary layer mixing schemes in the UK Meteorological Office Unified Model, paper presented at the ECMWF/GCSS Workshop on Parameterisation of the Cloud-Topped Boundary Layer, Eur. Centre for Medium-Range Weather Forecasts, Reading, U. K.
- Solomon, S., D. Qin, M. Manning, Z. Chen, M. Marquis, K. B. Averyt, M. Tignor, and H. L. Miller (2007), *Climate Change 2007: The Physical Science Basis: Contribution of Working Group I to the Fourth Assessment Report of the Intergovernmental Panel on Climate Change*, edited by D. Q. S. Solomon et al., 996 pp., Cambridge Univ. Press, Cambridge, U. K.
- Stott, P. A., D. A. Stone, and M. R. Allen (2004), Human contribution to the European heatwave of 2003, *Nature*, 432(7017), 610–614, doi:10.1038/nature03089.
- Taha, H., S. Konopacki, and S. Gabersek (1999), Impacts of large-scale surface modifications on meteorological conditions and energy use: A 10-region modeling study, *Theor. Appl. Climatol.*, 62(3–4), 175–185, doi:10.1007/s007040050082.
- Trenberth, K. E., D. P. Stepaniak, and J. M. Caron (2000), The global monsoon as seen through the divergent atmospheric circulation, *J. Clim.*, 13(22), 3969–3993, doi:10.1175/1520-0442(2000)013<3969:TGMAST>2.0.CO;2.
- Uddin, M. N., and D. R. Marshall (1988), Variation in epicuticular wax content in wheat, *Euphytica*, 38(1), 3–9, doi:10.1007/BF00024805.
- Weaver, A. J., K. Zickfeld, A. Montenegro, and M. Eby (2007), Long term climate implications of 2050 emission reduction targets, *Geophys. Res. Lett.*, 34, L19703, doi:10.1029/2007GL031018.
- Wilson, M. F., and A. Henderson-Sellers (1985), A global archive of land cover and soils data for use in general-circulation climate models, *J. Climatol.*, 5(2), 119–143, doi:10.1002/joc.3370050202.
- Wiscombe, W. J., and S. G. Warren (1980), A model for the spectral albedo of snow. 1. Pure snow, *J. Atmos. Sci.*, 37(12), 2712–2733, doi:10.1175/1520-0469(1980)037<2712:AMFTSA>2.0.CO;2.

P. J. Irvine, D. J. Lunt, and A. Ridgwell, Bristol Research Initiative for the Dynamic Global Environment, School of Geographical Sciences, University of Bristol, University Road, Bristol BS8 1SS, UK. (p.j. irvine@bris.ac.uk)